Design And Development of a Lab-Scale Wildfire Ember Simulator

by

Aniruddh Sawant

B.Eng., Mumbai University, 2019

A Project Report Submitted in Partial Fulfillment of the
Requirements for the Degree of

MASTER OF ENGINEERING

in the Department of Electrical and Computer Engineering

©Aniruddh Sawant 2022

UNIVERSITY OF VICTORIA

All rights reserved. This report may not be reproduced in whole or in part, by photocopy or other means, without the permission of the author.

Design And Development of a Lab-Scale Wildfire Ember Simulator

by

Aniruddh Sawant

B.Eng., Mumbai University, 2019

Supervisory Committee

Dr. Ilamparithi Chelvan, Supervisor

(Department of Electrical and Computer Engineering)

Prof. Ashoka Bhat, Co-Supervisor

(Department of Electrical and Computer Engineering)

Abstract

Wildfires can be caused by natural phenomena like lightning or can be man-made. This fire can spread rapidly destroying forests and urban wildlands. One of the main causes for the spread of wildfires is embers or firebrands. The small and lightweight embers are capable of travelling long distances. When these embers land and accumulate on flammable surfaces they ignite them causing injury, death and financial losses. These losses can be reduced by residents living near forest fire prone areas if they are made aware of the destructive effects of embers and if safety precautions are followed. This project presents a laboratory scale prototype of a simulator capable of projecting simulated ember materials onto a model house. The goal of projecting these simulated embers is to determine areas in and around the house where there is a chance for embers to accumulate. This gives an idea to residents to keep these areas free from materials that can catch fire. The simulator discussed in this report uses a centrifugal blower of 440 CFM to shower ember materials on a house whose dimensions are scaled down to 6 ft x 3 ft x 6 ft (l x w x h). Thermocol, paper and woollen balls are tested as fake ember materials. It is found that the range and height covered by woollen balls are more than the other two. The average horizontal and vertical distances covered by the woollen balls when the blower was inclined at 45° is found to be 12 ft and 6 ft respectively. In the prototype, the ember materials are fed from a storage tank mounted to the blower output using a feeding mechanism. This ember simulator is mounted on a chassis, which is driven by four DC motors. Two of the motors have integrated encoder modules. The readings from these encoders were used to make the chassis move in a straight line. As a result, the prototype simulator is able to project ember materials on a model house while moving in a straight line.

Table of Contents

List of Figures

List of Tables

Acknowledgements

I acknowledge the generous financial support from the Wighton Engineering Product Development Fund.

I would like to thank my supervisor Dr. Ilamparithi for his patience, guidance and suggestions throughout my MEng journey. I am grateful to my co-supervisor Prof. Bhat for his time serving as the supervisory committee member. Special thanks to Kelsey Winter and Mike Kimmerly from FireSmart BC for their support throughout the project by giving the needed direction.

I would also like to thank the laboratory technicians, Brent and Rob for their insights in building the prototype. Also, I thank my lab-mate Dr. Praneydeep Rastogi who helped me perform several tests and collect the infinite wool balls that were dispersed in the lab.

More importantly, I am eternally grateful to my parents and two sisters for their love, support and encouragement throughout my life.

Chapter 1

Introduction

1.1. Background

In this project, the design of a lab-scale prototype of a wildfire ember simulator is discussed. Wildfire is an uncontrolled fire that can burn in forests, grasslands, savannas and other ecosystems [1]. They are not limited to a particular continent or environment and often occur in rural areas. Wildfires can burn in vegetation located both in and above the soil. The cause of a wildfire can be a natural occurrence—such as a lightning strike—or a human-made spark [2-5]. From 1959 to 2015, wildfires have burned 1.96 Mha per year in Canada and the annual area burned is trending upward [2]. In BC, 868,203 hectares of land was burned by 1,610 wildfires from April 1, 2021 to September 30, 2021. Around 35% of these wildfires were man-made and 60% were acts of nature and the cause of the remaining 5% is unknown [6].

The weather conditions and environment determine how much a wildfire can grow. The main reason for the spread of wildfire are fire embers. Forest fires create embers, which are small firebrands, pieces of superheated wood and other material. They can travel a large distance from their source with the help of wind as they are lightweight. These embers are capable of causing fire if they land on flammable materials like dry or dead plants or on flammable infrastructure and ignite them. If the forest fire is huge, it can generate thousands of such embers, also known as an ember storm.

Buildings and homes that lie within the path of a wildfire are destroyed, which not only cause financial losses but also expose hazardous materials posing threat to human health. The 2017 British Columbia fires spread to 1.2 million hectares [6, 7]. The losses

resulting from forest fires are reported in [8]. The financial damage because of the 2003 Kelowna wildfires in British Columbia was $252 million. It was about $864.67 million in the 2011 Slave Lake wildfires Alberta. The 2016 Horse River Wildfire in northeastern Alberta reported $3.84 billion in damages, which is the costliest natural disaster in Canadian history. Reference [9] reported fire statistics for 2019/20 in Australia where the total burned area was 18 Mha with 3,113 houses lost. According to [10], there were 85 fatalities and around 19,000 structures destroyed in the 2018 Campfire in the USA. From [11], it is known that as many as 90% of homes and buildings were damaged or destroyed because of fires started by embers. Therefore, it is important to draw attention towards the effects caused by flying embers.

1.2 FireSmart BC

The British Columbia (BC) FireSmart Committee, composed of a group of agencies, directs a FireSmart program [12]. The goal of FireSmart in BC is to come up with plans that help support wildfire preparedness, prevention and mitigation in BC. In order to communicate the risks caused by ember ignition, FireSmart BC planned to design a portable wildfire ember simulator. This simulator would project a substance onto a house. This substance, the ember simulant, would have the same dimensions and weight as a wildfire ember and would be such that it can be easily spotted. Additionally, the selected fake ember material should be such that it can be easily washed away or collected from the experimented field after the demonstration. The aim of designing this simulator would be to create an ember storm using the ember simulant, project it on a house and observe places where it could possibly accumulate and cause a fire. This will help raise awareness to individual property owners near wildfire prone areas about maintaining their property to reduce the risk of wildfire spread.

1.3 Dimensions of the Model House

According to the residential development standards A3 and B6 for street setbacks, the distance from a residential house to street ranges from 2 m to 9 m (~30 ft) and the maximum height of a building according to standards A4 and B7 can be 9 m (~30 ft) [13, 14]. So, the fake embers projected from the simulator should be able to cover a horizontal and vertical distance of around 30 ft. For the prototype designed and discussed in this report the model house as shown in Fig. 1.1. has dimensions that are scaled down by a factor of 5. That is, the height of the house and distance of the house from the blower prototype is 6 ft. The prototype will be showering the simulated ember across 3 ft width of the house. This distance can be increased or decreased depending on the width of the house.

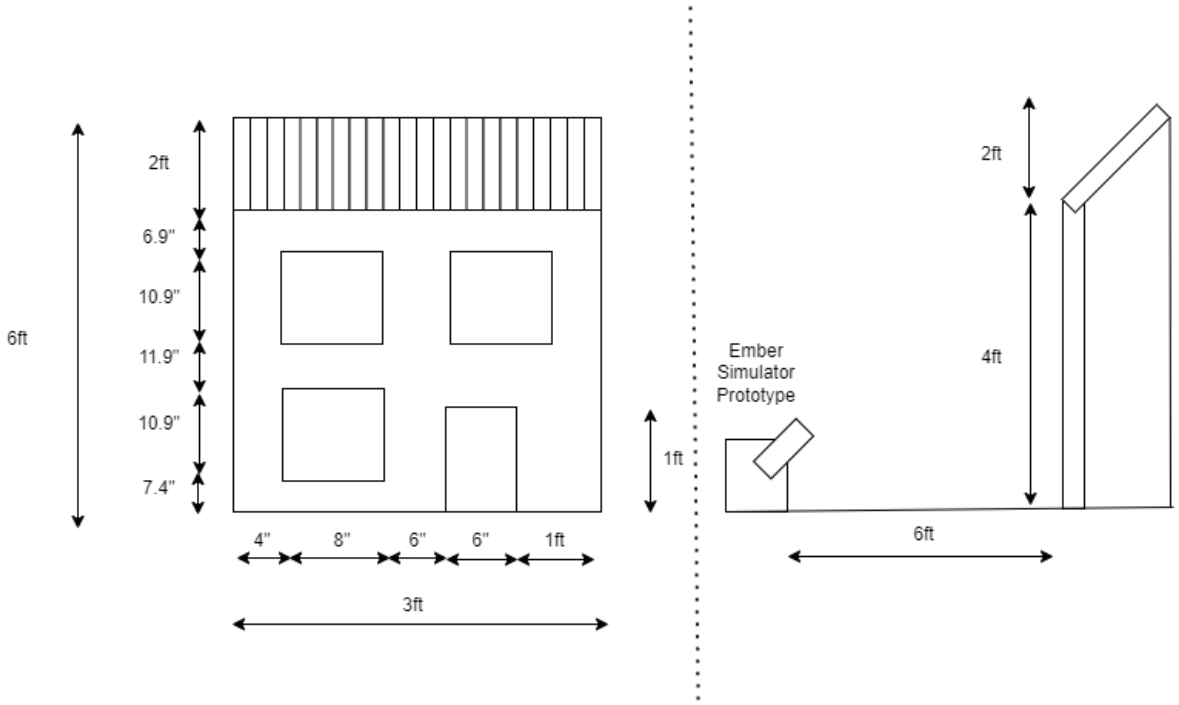

Fig. 1.1. Model house dimensions

1.4 Characteristics of Embers

The size and mass of firebrands created in wildfires have been studied and similar results have been produced in laboratories. Reference [15] determined the size of firebrands from the holes that were generated in a trampoline wall by firebrands during the Angora Fire in California. The trampoline wall was 9.8 m from an affected house which had a distance of less than 1 mile downwind from the area of forest fire. The holes in this wall had an area less than 50 mm^2. Additionally, upon inspection of 212 locations, it was found that the majority of the holes had an area of less than 40 mm^2. This shows that such small firebrands are also capable of causing fire. More than 90% of the firebrands measured in the fires generated in the Bastrop County Complex Fire site in Texas had an area less than 50 mm^2 and more than 85% were less than 5 mm^2 [16]. Reference [17] reported approximately 80% of the total firebrands had a cross sectional area around 50 mm^2 to 200 mm^2 having a mass range of 10-20 mg. Reference [18] found that cylindrical firebrands had diameters ranging from 1 to 6 mm and the majority of the firebrands weighed between 5 mg and 20 mg.

In laboratory-scale experiments, [19] reported that 83% of the collected firebrands produced by burning 2.6 m Douglas fir trees had surface area of less than 1000 mm^2 and mass less than 0.3 g with largest mass in the range of 2.1 g to 2.3 g. Later, in a similar work performed by [20] with Korean pine, it was observed that a large percentage of the firebrands had a mass of less than 0.3 g and a majority of them had a surface area of less than 1000 mm^2. In another study, [21] used the National Institute of Standards and Technology (NIST) Dragon to determine the characteristics of embers produced from the Ponderosa pine trees. The cylindrical embers had diameters from 8-12.5 mm, length of around 50 mm and weighed less than 0.2 g.

1.5 Objectives of this Project

The objectives of this project are:

1) Select a material to be used as the ember simulant.
2) Design an ember projecting mechanism.
3) Mount the projecting mechanism on a chassis that can move in a straight line.
4) Create an ember storm and project ember simulants on a scaled down model house.

1.6 Organization of the Report

This report is organized as follows:

Chapter 1 gives an overview of the project specifying the goals to be accomplished.

Chapter 2 reviews various ember simulators reported in literature and proposes a design suitable for the project under consideration.

Chapter 3 provides information about the tests performed using two ember blowing mechanisms to select the fake ember. It also presents the results of height achieved by the selected ember material and blowing mechanism.

Chapter 4 describes the mechanism used to carry the blowing apparatus.

Chapter 5 concludes the report with some remarks and suggestions to improve the design.

Chapter 2

Ember Simulator

2.1. Ember Simulator Design

As discussed in Chapter 1 embers are a great threat and are one of the major factors contributing to the spread of wildfire. Hence, it is important to test the effects of embers and to scope its impact on the natural and urban environment. To do the same, several firebrand simulators have been designed. These simulators have many applications from studying characteristics of ember to studying the role of ember in igniting different materials used in building houses. These simulators are capable of producing fire embers of different sizes and in some studies [21-23] these simulators were used to study sizes of embers created by different types of trees. To study its impact on urban wildland, the ember simulators were also used on model houses and parts of model houses [22, 24, 25]. The model houses designed for these studies followed constructional codes and regulations mandated in wildfire prone areas so as to study the intrusion of firebrands in these model houses.

The aim of this project is to study the accumulation of embers on houses and its surrounding area specifically in wildfire prone regions. To do this, there is no need to create actual embers and risk starting fires. Non-flammable materials having the same characteristics like mass, dimensions can be used to demonstrate this. Although the ember simulators designed so far can only create actual embers unlike the aim of this project, their designs can be studied in order to develop a mechanism that shoots the fake embers. This is because even if it is planned not to create actual embers, the characteristics of the embers to

be projected are the same as that of actual embers. To study how the embers are projected, the design of some popular ember simulators are discussed below.

In [21], a firebrand generator was developed as shown in Fig. 2.1. under the National Institute of Standards and Technology (NIST). The NIST Dragon produces firebrands of different sizes as in an actual wildfire. The generator consists of a blower connected to a vertical pipe. This vertical pipe can be disassembled to load wood pieces on a wire mesh surface. The loaded wood pieces are burnt using two propane burners. A line for these burners is made below the wire mesh. When the wood pieces are loaded, another vertical pipe is mounted which acts as an outlet for the firebrand generator. This pipe allows the generated firebrand to be projected in the desired direction. Once the top section of the vertical pipe is properly mounted, the blower and the burners are turned on. The air generated by the blower pushes the firebrands out through the pipe. The projected firebrands were collected by 157 rectangular pans placed in front of the firebrand over a distance of 1130 cm.

In [22] another firebrand generator for small scale testing in a laboratory called the NIST Baby Dragon is reported. Similar to the NIST Dragon, the Baby Dragon too has a blower to generate firebrands. In addition to that, a wind tunnel is used to generate different wind speeds upto 10 m/s. The generated firebrands enter the wind tunnel and are pushed by the air produced by the axial fan. The aim of designing this simulator was to test the firebrand penetration into vents protected by screens. This design as compared to the NIST Dragon allows generation of different wind speeds, which is an important parameter in ember storm generation. Along with this, it also allows to load the feed used to generate firebrand continuously as opposed to the NIST Dragon where this was not possible.

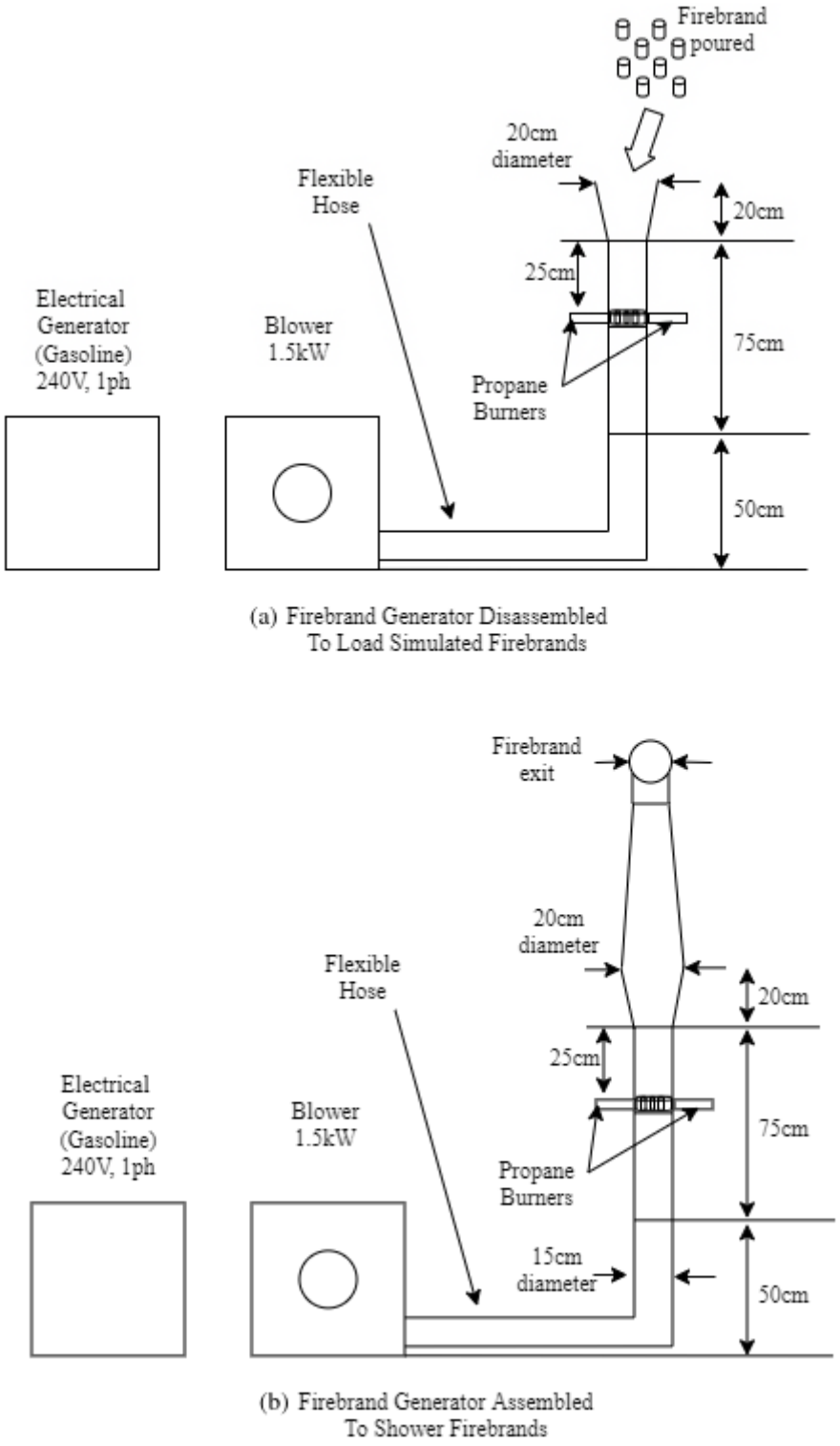

Fig. 2.1. Schematic of firebrand generator by Manzello [22]

Reference [23] designed a similar firebrand generator as shown in Fig. 2.2. This mechanism was designed to solve the issue of reverse ember flow in the NIST Baby Dragon

that would scatter firebrands in the laboratory making it dangerous for people using the generator. To address this, the authors added a splitter in the pipe that connected the wind tunnel. This design eliminated the use of a blower to generate the embers. Moreover, a significant reduction in the reverse ember flow was observed. The maximum wind speed observed was around 21 m/s. This wind speed was generated and varied by the axial fan in the wind tunnel. This is achieved by flaps present at the tip of the splitter which can be bolted on different heights. These flaps control the amount of air that passes through the generator, hence, controlling the wind speed inside the generator.

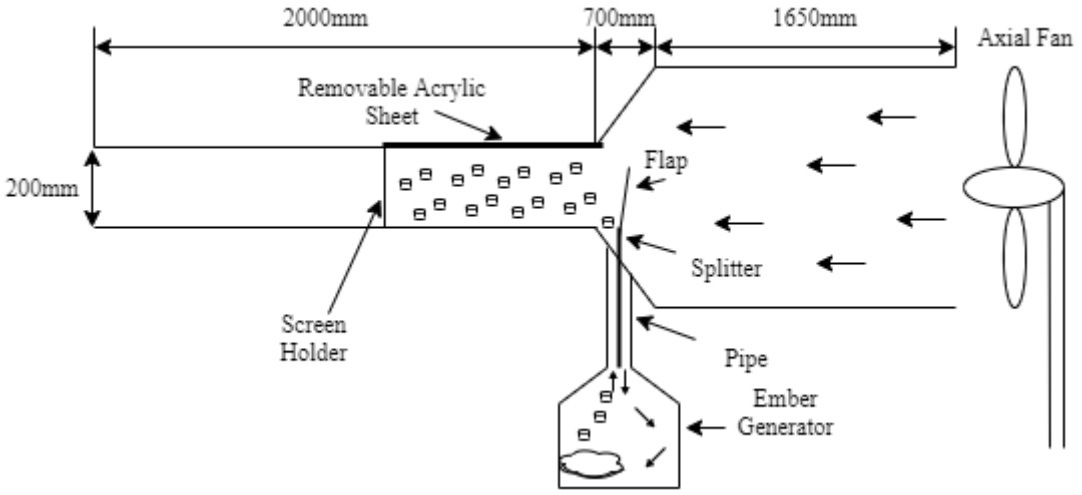

Fig. 2.2. Schematic of Ember Simulator by Sharifian [23]

2.2. Prototype Design

A blower fan is a common component in the simulators described above. The most important parameter of a blower fan is the air flow capacity of a fan. The amount of air a fan can displace per unit time is the air flow capacity of that fan. It is commonly expressed as cubic feet per minute (CFM). To define the parameters of the fan to be used for the prototype

to be designed, it is crucial to know the distance and height that is to be covered by the projected ember materials.

The maximum air flow capacity of a fan is given by,

$$Q = v*A \ldots.(m^3/s) \quad (2.1)$$

where Q is the maximum airflow capacity, v is the velocity of air and A is the area of cross section of the blower outlet. The ember material will be projected with the velocity of air produced at the outlet. That is, the initial velocity of ember simulant is the same as the outlet blower velocity. Since, the height and range to be covered by the ember material is known, its projectile motion can be analyzed and the initial velocity can be estimated. This value of velocity can then be used to calculate the air flow capacity of the blower fan to be used. It is well known that the trajectory of a two dimensional projectile is a parabola. However in the analysis of a two dimensional projectile, several parameters like air resistance, mass of the object in projectile, constant acceleration due to gravity, etc. are not considered and their effects have been previously studied and analyzed [26-30].

Reference [31] used an analytical approach to investigate the projectile motion of a spherical object in a medium with quadratic drag force. The table below from [31] shows a comparison of analytical formulae used to calculate parameters of a projectile motion with and without drag force. In the Table 2.1, R is the drag force, m is the mass of the object, g is acceleration due to gravity, k is the proportionality constant for calculating the drag force, v is the initial velocity, h is the maximum height of ascent, θ is the angle of projection, l is the range, v_a is the velocity in the x-direction and t is the motion time.

Table 2.1. Comparison of Analytical Formulae of Projectile Motion [31]

No drag ($R = 0$)	Quadratic drag force ($R = mgkv^2$)	SI Unit
$h = \frac{v^2 sin^2\theta}{2g}$	$h = \frac{v^2 sin^2\theta}{g(2 + kv^2 sin\theta))}$	m
$t = 2\sqrt{\frac{2h}{g}}$	$t = 2\sqrt{\frac{2h}{g}}$	s
$v_a = vcos\theta$	$v_a = \frac{vcos\theta}{\sqrt{1 + kv^2(sin\theta + cos^2\theta ln tan(\frac{\theta}{2} + \frac{\pi}{4}))}}$	m/s
$l = v_a t$	$l = v_a t$	m

The constant k is given by,

$$k = \frac{\rho_a c_d S}{2mg} s^2/m^2 \tag{2.2}$$

where, ρ_a is the density of air (1.225 kg/m^3), and c_d and S are the drag coefficient and the area of cross section of the object in projectile respectively. From section 1.4, the mass of ember is known to be less than 0.2 g with a cross-sectional area of around 50 mm^2. For calculating k, let the mass of a spherical ember simulant of diameter 1 cm be 0.1 g.

Substituting, h = 1.82 m, g = 9.81m/s^2, c_d(sphere) = 0.5, S = 78 mm^2 = 7.8 x 10^{-5} m^2 , θ = 45^o and m = 0.1 g = 0.0001 kg in (2.2), the value of k is found to be

k = 0.02441 s^2/m^2

Now, the initial velocity calculated from the Table 2.1. as shown in (2.3) is,

$$v = \sqrt{\frac{2hg}{sin^2\theta - hksin\theta}} \tag{2.3}$$

v = 13.72 m/s

The initial velocity in the x-direction and the motion time are calculated to be v_a = 3.88 m/s and t = 1.21 s from Table 2.1. So, the expected range of the object is,

$$l = v_a * t \quad (2.4)$$

= 4.72 m (~15 ft)

The maximum air flow capacity of the blower needed to achieve the maximum height and range can be calculated from (2.1), where the diameter of the blower outlet is assumed to be 4", i.e area of cross section, A = 0.0081 m^2

$Q = v*A$

Q = 0.1112 $m^3/s \approx$ 235 CFM

From the above calculations, it is estimated that a blower of around 235 CFM should set spherical ember simulants of 0.1 g mass with 1 cm diameter in a projectile that covers a range of around 15 ft and a maximum height of 6 ft.

2.3 Prototype Blower Specifications

Centrifugal fans are capable of generating relatively high pressures. The air enters the impeller axially and is discharged outside in a centrifugal direction, hence they are called centrifugal fans. The design of a basic centrifugal fan is as shown in Fig. 2.3. The air is sucked in by the impeller via the inlet. The impeller moves the axially entered air through the blades. Generally, centrifugal fans have three types of blades - forward blades, backward blades and radial blades. The impeller is mounted in a casing with an outlet from a scroll casing 90 degrees from the inlet. As a result, the air leaves the outlet radially [32].

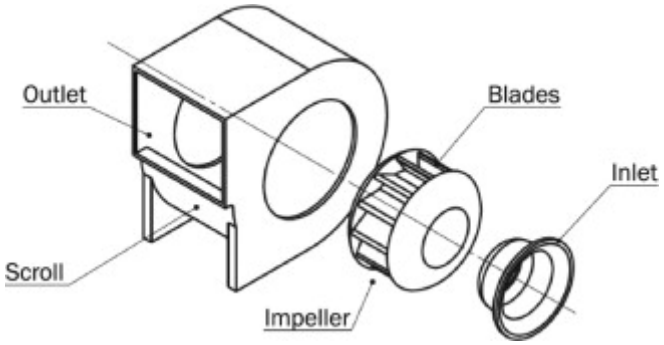

Fig. 2.3. Parts of a Centrifugal Fan [32]

Table 2.2. Specifications of the SPX Johnson Centrifugal Pump

Specifications	
Length	150 mm
Width	257 mm
Height	290 mm
Inlet Diameter	150 mm
Outlet Diameter	130 mm
Maximum air flow capacity	440 ft^3/m
Voltage	12 V DC
Power rating	250 W

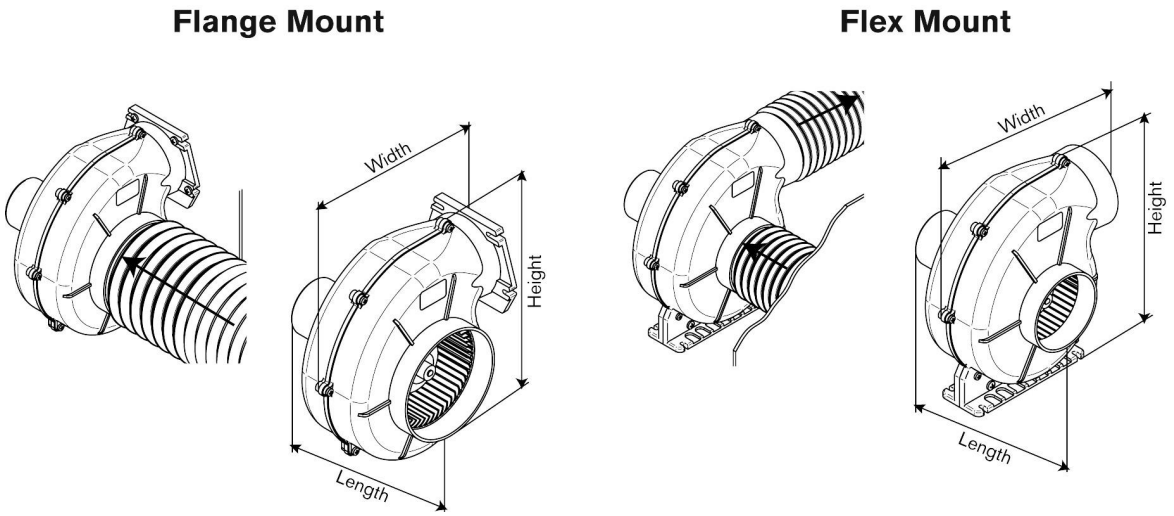

Fig. 2.4. SPX Johnson Blower- Flange and Flex Mount [34]

To test the calculations, a centrifugal fan - SPX Johnson Centrifugal Pump was used as shown in Fig. 2.4. The specifications of the fan are shown in Table 2.2. The dimensions of the fan are 150 mm x 257 mm x 290 mm (l x w x h) [34]. It is a 12 V DC fan with a power rating of 250 W and consumes a peak current of around 20 A. The inlet diameter is 152.4 mm (6”) and the outlet diameter is 101.6 mm (4”). The maximum air flow capacity is 440 CFM. The air flow capacity of the fan can be controlled by changing the voltage supplied to the blower.

To check the height and range achieved by the blower a woollen/cloth ball was used. This spherical cloth ball had a diameter of 1cm and weighed about 0.1 g. The blower was inclined at an angle of 45 deg. The blower was turned on by a DC supply whose voltage was slowly increased. The wind speed produced by the blower was measured using an anemometer. The wind speed increased as the blower voltage was increased and it was observed that at 6.8 V the blower produced a wind speed of 13.7 m/s. The cloth ball was dropped manually directly in front of the blower outlet and this was repeated 10 times to get the average distance covered by the balls. As expected, the ember materials were set in a projectile motion. The distance covered by these materials was measured manually and is shown in Fig. 2.5. below:

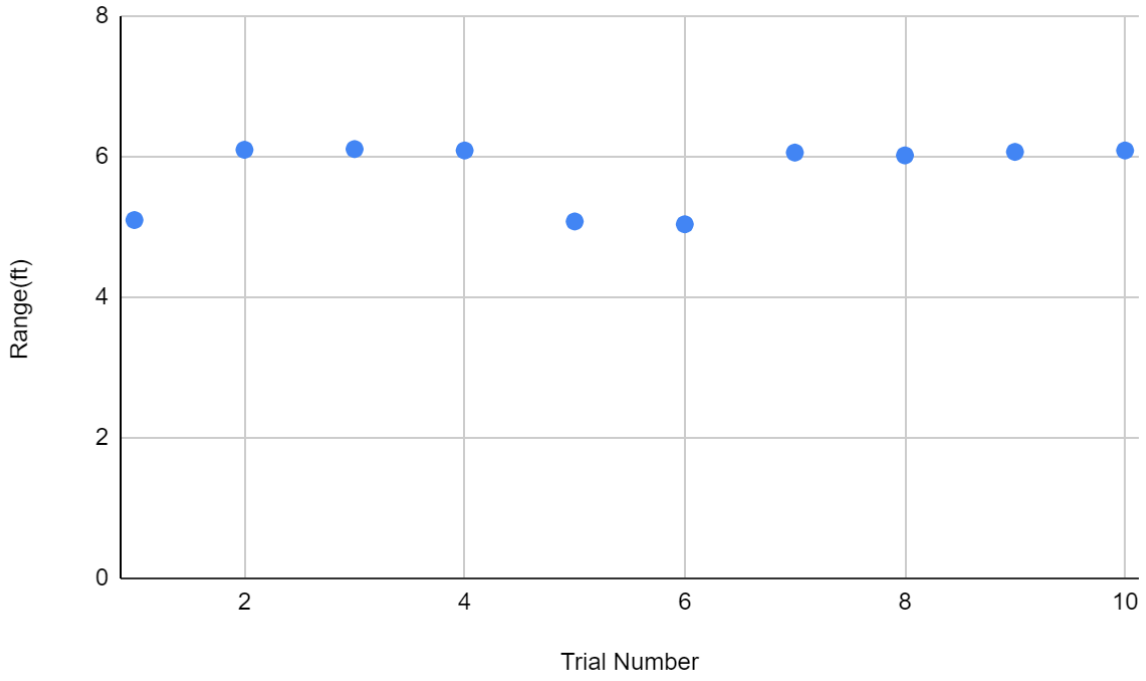

Fig. 2.5. Scatter plot of range at 6.8 V blower voltage

The average distance covered by the cloth balls was 6’4” which is less than the calculated range value. The prototype is planned to project ember materials 6 ft from the model house and the height achieved by the materials should be 6 ft. To check this, the blower was kept 6 ft from a wall and was turned on by supplying 6.8 V to produce a wind speed of 13.7 m/s. The cloth balls were dropped in front of the blower outlet and the point of contacts on the wall were marked. The vertical distance from the ground to these points were measured. The 10 readings observed are shown in Fig. 2.6. below. The average height measured from the ground is around 2’10”, which is not desirable. It is important to note that this height measured is not the maximum height of the projectile, rather it is the height that is achieved when the prototype is placed 6 ft away from the wall.

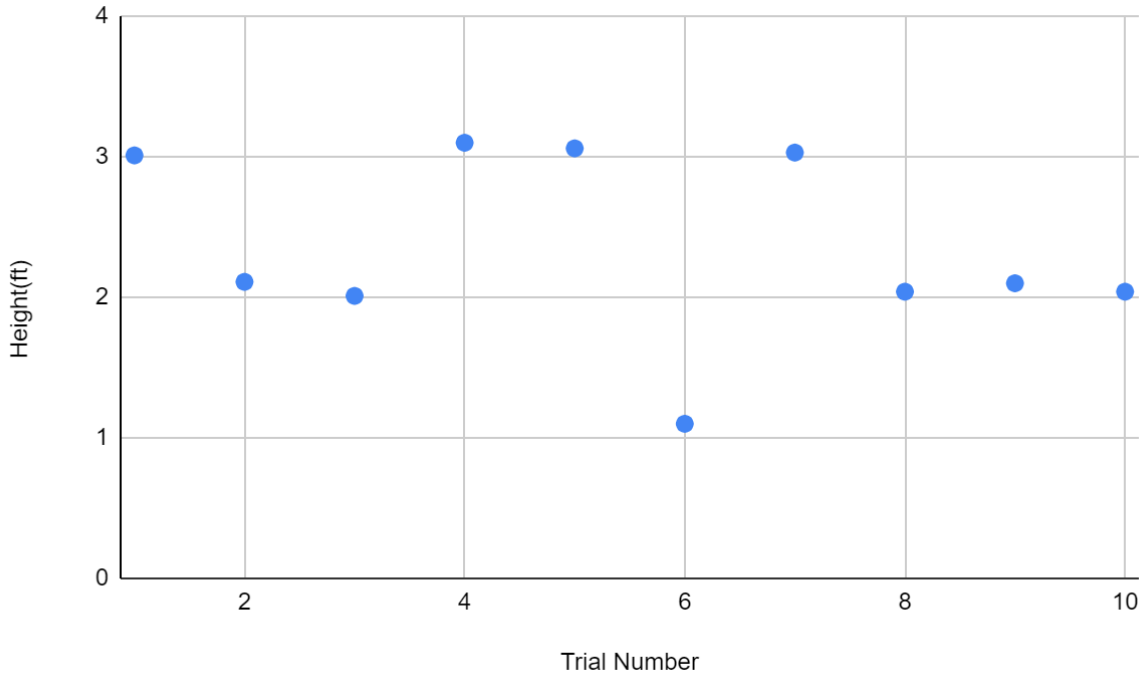

Fig. 2.6. Scatter plot of height at 6.8 V blower voltage

To rectify this, the blower voltage was increased to 12 V in order to increase the air speed at the outlet of the blower and the same experiment was performed again. The wind speed was measured with an anemometer which produced a reading of 21 m/s. Again with the same setup, the cloth balls were dropped in front of the blower and the range covered and the vertical distance when the blower was kept 6 ft away from a wall were measured. The 10 readings of each of these tests are shown in Fig. 2.7. and Fig. 2.8. below:

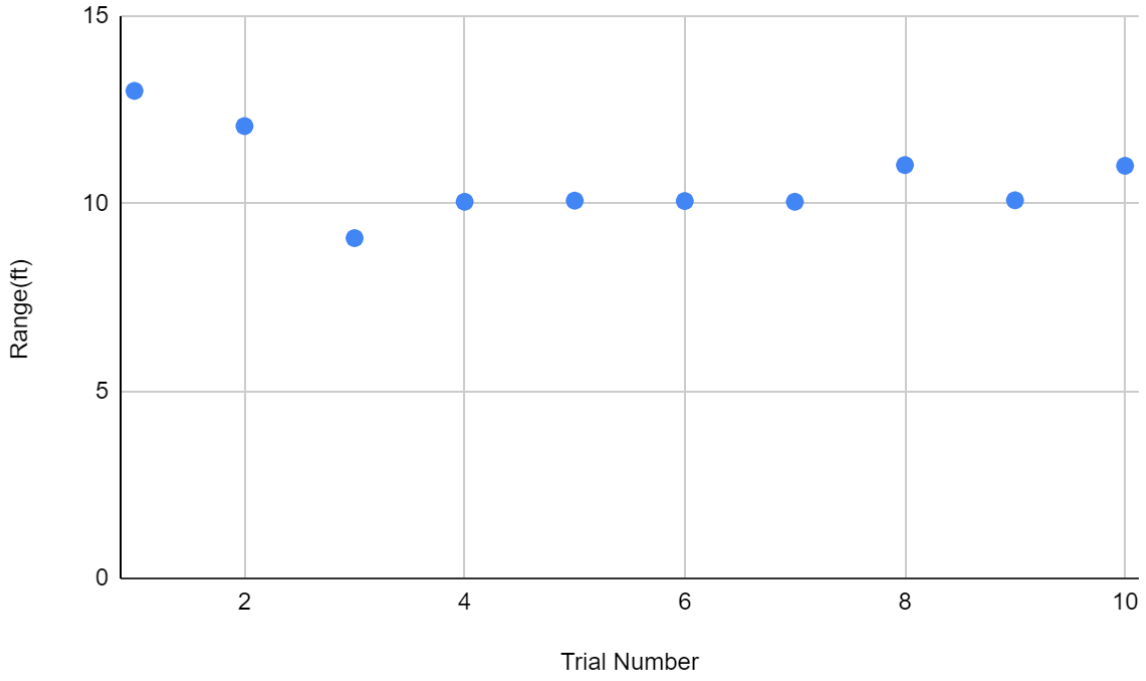

Fig. 2.7. Scatter plot of range at 12 V blower voltage

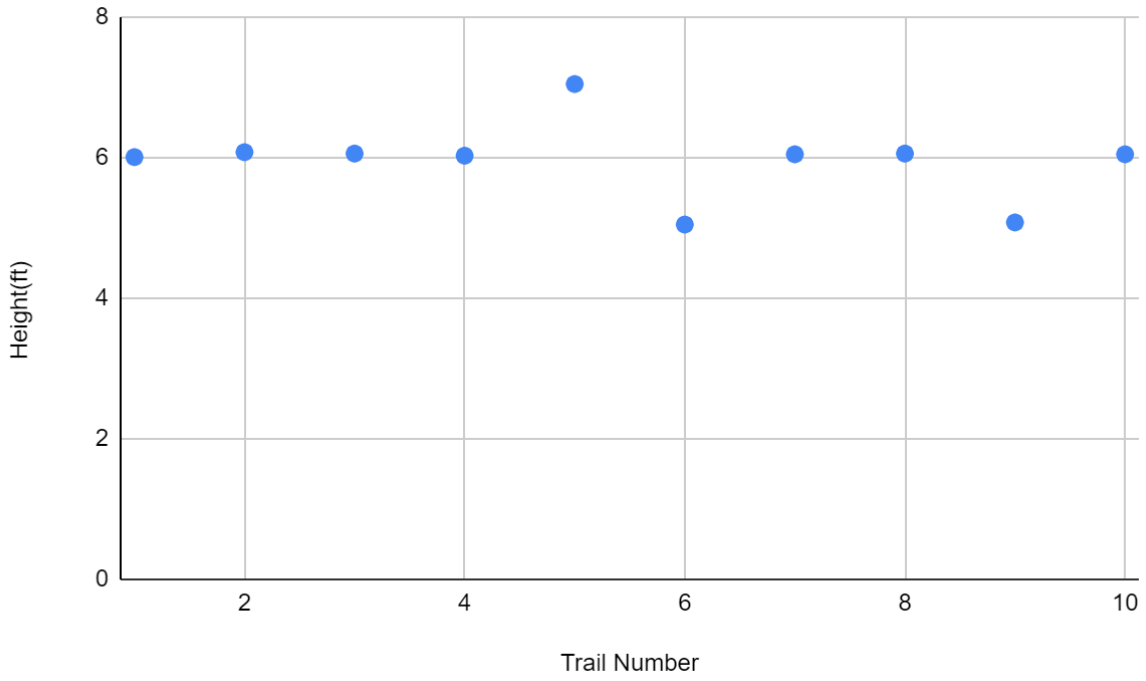

Fig. 2.8. Scatter plot of height at 12 V blower voltage

From the plots shown in Fig. 8 and 9, the average range covered is observed to be around 11’ and the average height produced by the blower when kept 6’ from the wall is

6’4”. With these results, we can conclude that the blower is capable of projecting the ember materials to the estimated height of 6 ft when placed at a distance of 6 ft.

The readings in the above tests were of cloth balls manually dropped at the blower outlet. In the next chapter, the design of the ember simulator is presented. Moreover, tests carried out to select ember material and the range and height achieved by different materials are discussed.

Chapter 3

Selecting Ember Simulant and Prototype Design

3.1 Selecting Ember Simulant

From Chapter 1, the size of embers observed in different studies was around 50 mm^2 with weight less than 0.2 g. The ember material to be used as a simulant too should have these characteristics. Keeping these parameters in mind, three materials were decided to be tested- styrofoam/thermocol balls, paper balls and wool/cloth balls. Their characteristics are listed in Table 3.1. Out of these materials, even though thermocol is a non-biodegradable material and paper is a flammable material, they were decided to be experimented with because of some of the properties they possess. Thermocol balls when projected follow a random and unpredicted trajectory, quite similar to embers. As for paper balls, they are available readily and an alternative like non-flammable or flame retardant paper can be used instead of a normal paper. Wool balls on the other hand are lightweight, can be made of various sizes, biodegradable, and non-flammable but costs more as compared to the other two. There are advantages and disadvantages of using these materials.

Table 3.1. Characteristics of Ember Simulant

	Non-flammable	**Biodegradable**	**Easy-to-collect**	**Cost**
Styrofoam	No	No	Yes	Inexpensive
Paper	No	Yes	Yes	Inexpensive
Wool	Yes	Yes	Yes	Expensive

Having said that, all of the above discussed materials can be easily used for simulating an ember shower in a lab environment similar to [35]. The results and observations of tests conducted with each material are discussed in the section below. The

following tests will help in selecting the ember material for the prototype and in determining the maximum range covered by each tested ember material.

3.2 Setup for selecting ember simulant

The prototype to be designed should be able to project the ember materials discussed above. To address the problem statement, the setup discussed below was implemented. This setup has similar implementation as the previously reported ember simulators. The basic idea of the prototype is that the ember materials will be dropped by a feeding mechanism in the path of the blower's outlet. This will project the ember materials in a trajectory covering a range. For selecting the ember material, distance covered by different testing materials is important because in the final implementation the simulator should be able to shower the ember materials from the road. The angle of the blower mechanism can then be adjusted to target different portions of the house. Different experimental setups designed to select the ember material are described below.

3.2.1 First Prototype

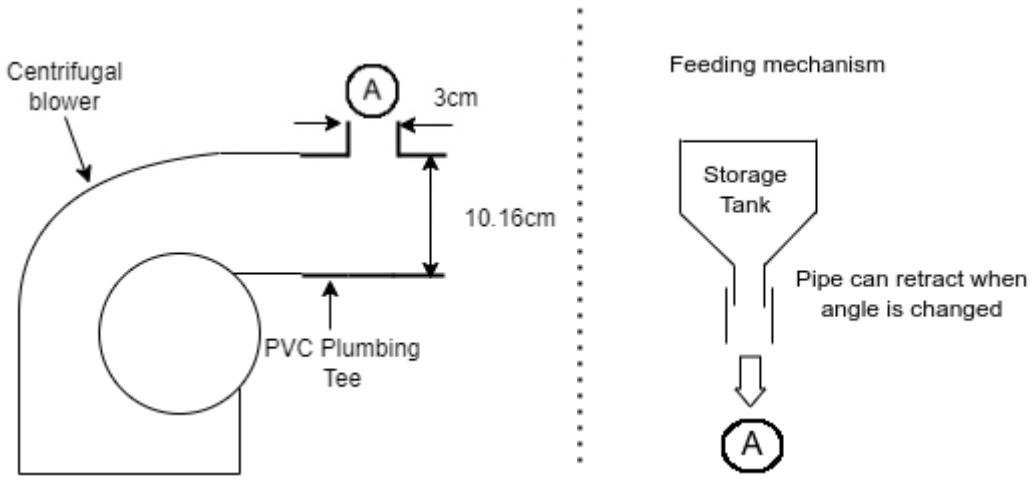

Fig. 3.1. Blower with Plumbing PVC Tee outlet and Feeding Mechanism

The first test was performed by connecting a 10.16 cm (4”) diameter plumbing tee joint to the outlet of the blower as shown in Fig. 3.1. A tee joint was used so as to input ember materials through the top inlet of the tee joint. This setup was experimented with three types of ember materials - styrofoam, paper and cloth balls. The ember materials were fed to the blower by a feeding mechanism. The feeding mechanism as shown in Fig. 3.1. contains a storage tank where ember materials to be projected are stored. This storage tank is mounted on the same structure as the blower. The storage tank as shown in Fig. 3.1. was designed to allow all ember material to pass through without creating a blockade. A pipe was connected from the outlet of the tank to the outlet of the blower. If the storage tank is loaded before turning on the blower, it was found that ember balls accumulate at the outlet of the blower. In the future, a valve controlled mechanism can be designed to open and close the pipe. So, the storage tank was loaded after turning on the blower. The blower was inclined at an angle of 45 degrees and turned on by supplying a voltage of 12 V. At first, the wind speed produced by the blower was measured using an anemometer. The digital anemometer was placed at the output of the blower. The measured wind speed was measured as 17.4 m/s. The ember balls were then dropped one by one and the distance covered was measured manually. This was done by marking the spot where the ember landed and then measuring the distance from the blower to that spot using a measuring tape. 30 trials of thermocol, paper and cloth balls each were taken. The average, standard deviation and variance of the distance covered by different ember materials is given below in Table 3.2. A scatter plot of the measured distance versus the sample number is shown in Fig. 3.2.

The scatter plot shows the distance covered by each material projected by the prototype. For instance, the average distance achieved with thermocol balls is 4’06” and the

plot shows that the distance covered by the thermocol balls has high variation. But, the average distance covered by these balls is too small. Even though randomness is preferred, the range in which the results are produced should be predictable. In case of thermocol balls, some balls fell 1’05” from the projected position while some covered around 8ft. On the other hand, cloth balls have a variance of 3’02” and the average distance covered is 11’07”, which is more than thermocol balls. Moreover, it is observed that most of the balls crossed more than 9” of distance from the blower. So, the randomness achieved with cloth balls falls in a certain range which allows to scale the randomness from 9” to 15”. The standard deviation of the distance achieved by using paper balls is 1’05”, i.e as compared to the other two ember materials paper balls produce consistent results and there is almost no randomness as compared to thermocol and cloth balls. From the plot, most of the paper balls lie around 10 ft which is an undesirable feature.

Table 3.2. Average, standard deviation and variance of distance covered by ember materials (Prototype 1)

Ember Material	Average distance	Standard Deviation	Variance
Thermocol	4’06”	2’04”	5’04”
Paper	10’02”	1’05”	1’08”
Cloth	11’07”	1’08”	3’02”

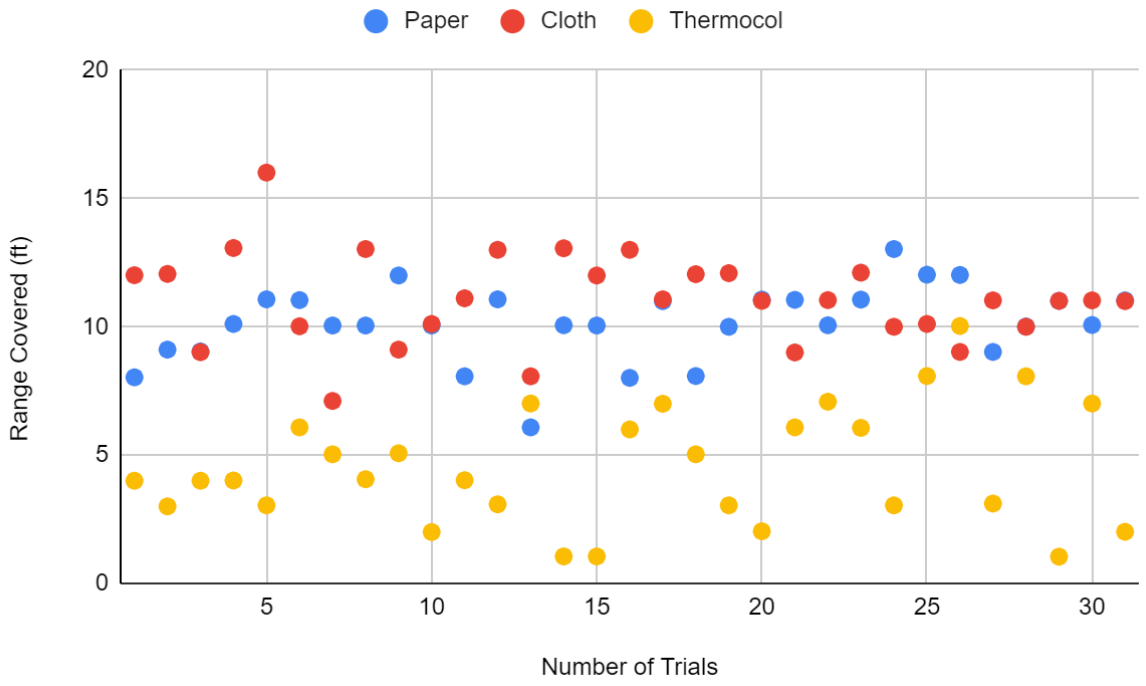

Fig. 3.2. Scatter plot of distance covered by ember materials

3.2.2 Second Prototype

From [25], the velocity can be increased by decreasing the outlet dimension. To achieve this, the structure shown in Fig. 3.3. was designed. This structure was connected to the outlet of the blower. The dimensions of the duct attached to the blower outlet are as shown in the same Fig. 3.3. The outlet diameter was decreased from 10.16 cm as implemented in the first test to 7.5 cm. The rest of the setup was kept the same.

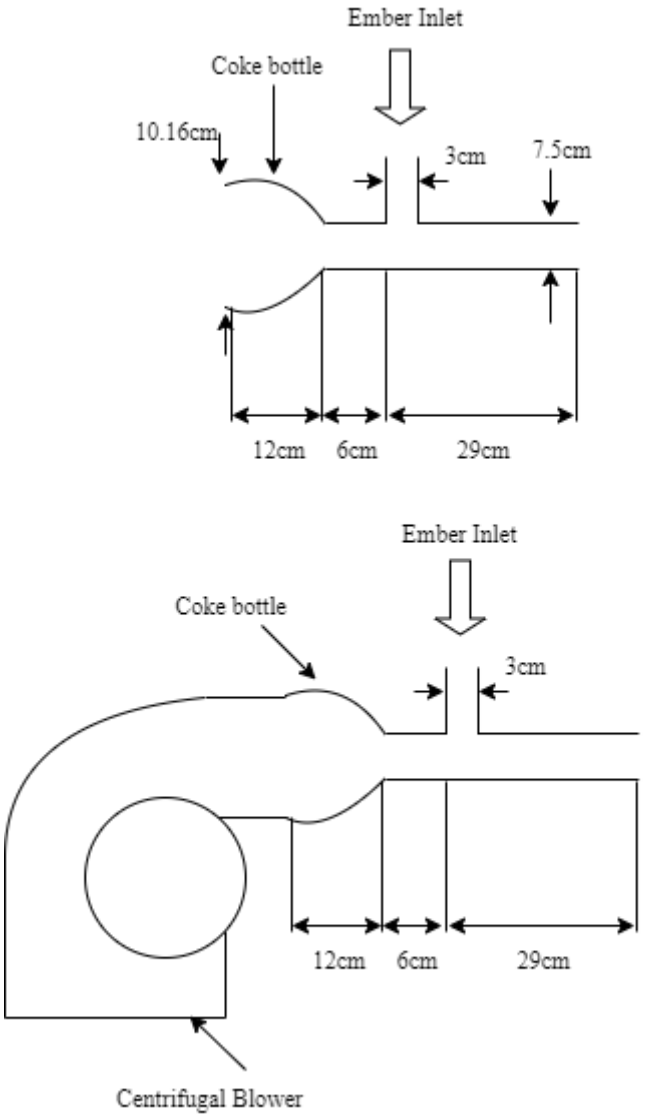

Fig. 3.3. Blower with reduced blower outlet dimensions

Table 3.3. Average, standard deviation and variance of distance covered by ember materials (Prototype 2)

Ember Material	Average distance	Standard Deviation	Variance
Thermocol	8’05”	2’09”	7’10”
Paper	12’10”	1’07”	2’09”
Cloth	12’05”	2’05”	6’02”

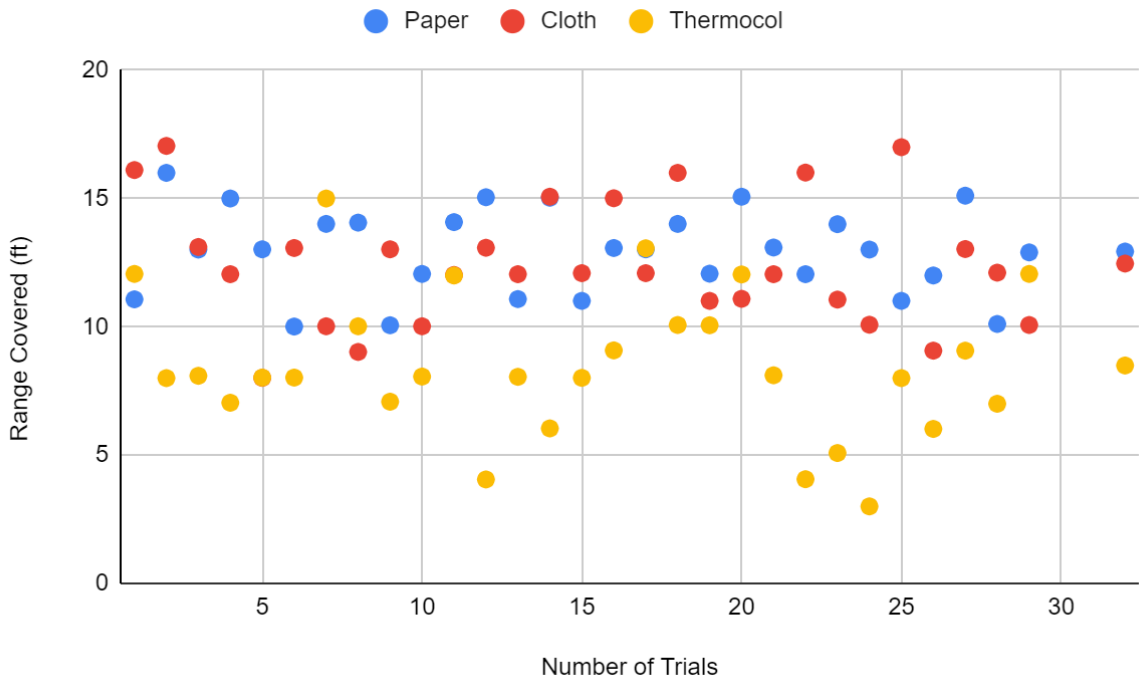

Fig. 3.4. Scatter plot of distance covered by ember materials

Similar to the previous test, the blower was inclined to an angle of 45 degrees. The wind speed produced by the blower was measured using an anemometer after turning the blower on by supplying 12 V. Upon placing the digital anemometer at the output of the newly designed output duct, a slight increase in the readings was observed. The measured wind speed was 19.2 m/s. On decreasing the duct size, the air loss at the feeding hole increased significantly. The wind speed measured at the feeding hole was 12.2 m/s. The ember balls were dropped into the feeding mechanism and the distance covered was measured manually. The same method was used to measure the distance covered by the ember materials. Again, 30 samples of thermocol, paper and cloth balls were taken and the average, standard deviation and variance of the distance covered by different ember materials was calculated and is shown in Table 3.3. The scatter plot of the measured distance versus the sample number is shown in Fig 3.4.

From Table 3.4. and Fig. 3.4., the average distance covered by the thermocol balls is 8’05”. As compared to the first test, the average distance covered by the thermocol balls has increased significantly. The plot shows a large number of samples around 8’05” and very few above 11’. That is, we can assume that the peak distance that can be achieved with thermocol balls is around 8’05”. On the other hand, even though cloth balls have a variance of 6’02”, the average distance covered is 12’05” which is more than thermocol balls. So, the randomness similar to thermocol balls is achieved and it is observed that it covers a greater distance than thermocol balls. Paper balls seem to produce consistent results as compared to the other two ember materials and for most samples covered a distance between 10’ to 15’. From the results, cloth balls showed promising results and are a good choice for the final simulator. The unpredictable nature of cloth ball’s projectile, ease of acquisition, availability of variable sizes and color concludes that it is a good solution for selecting the fake ember as its parameters are quite similar to actual embers.

3.3 Determining Height

For each trial the range covered by the same ember material is different. So, the maximum height of the projectile will also be different. In order to calculate the vertical distance, the blower apparatus was placed 6 ft from a wall. Similar to the above experiment, the blower was inclined at an angle of 45deg and was turned on by supplying 12 V. The readings were then noted by marking the point of contact on the wall and measuring the height from the ground using a measuring tape. This experiment was conducted only on cloth balls as it was finalized as the ember material to be used for the prototype.

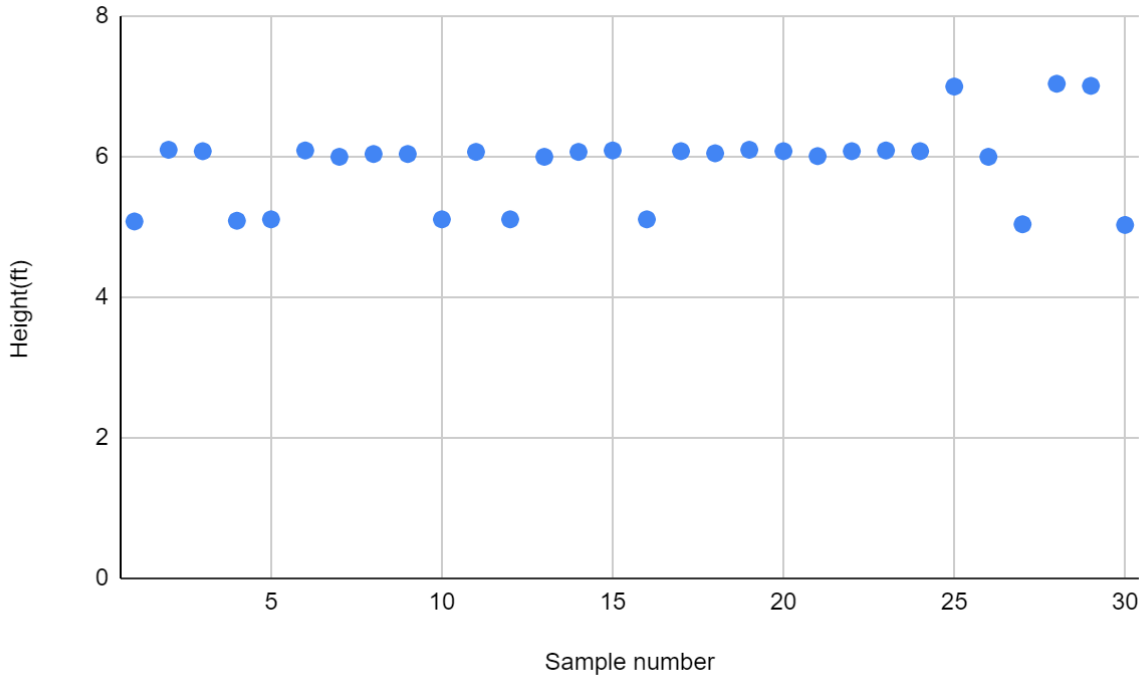

Fig. 3.5. Scatter plot of vertical distance covered by ember materials

Table 3.4. Average, standard deviation and variance of vertical distance

Average height	Standard Deviation	Variance
6’01”	0’06”	0’04”

Fig. 3.5. shows the scatter plot of vertical height of cloth balls measured from 30 trials. The cloth balls as shown in Fig. 3.5. and Table 3.4. collide at an average distance of 6’01” on the wall from the ground. As discussed in Chapter 2, the maximum height of the model house to be designed is 6 ft. For this model house, this blower apparatus will be able to project ember cloth balls on the roof of the house. By this experiment we can also conclude that the selected ember material is a good choice as a simulant for the prototype.

Chapter 4

Chassis of the Robot

4.1 Mechanism for carrying the blower

The blower apparatus is expected to automatically project the ember cloth balls across the width of the house. The implemented mechanism, an autonomous robot, is discussed below.

In this robot, a chassis is designed upon which the blower is mounted. This chassis is driven by DC motors and carries the weight of the blower and the storage tank loaded with the ember materials. The distance to be travelled by the robot, equal to the width of the house, can be input and the robot can travel in a straight line throwing the ember materials as it moves in front of the house. A prototype of this mechanism is implemented in this project and the components used to design this structure are discussed below.

4.2 Construction of the Chassis

The blower is mounted on a rectangular chassis of dimensions 50 cm x 20 cm. The length of the base of the blower is 15 cm. So, the width of the chassis was kept 20 cm as the blower is kept along the width of the blower. The chassis houses the blower, the feeding mechanism, the microcontroller and a switch which is easily accessible to turn off the chassis for safety. The chassis is driven by four wheels of 10 cm diameter which are run by four motors whose speed is reduced by gears. To house these components, the length of the chassis is kept at 50 cm. This setup is shown in Fig. 4.1. Cold rolled steel channels are used

to build this rectangular structure. The channels used are available in the Vex Robotics kit [36]. To drive this chassis four DC motors are used.

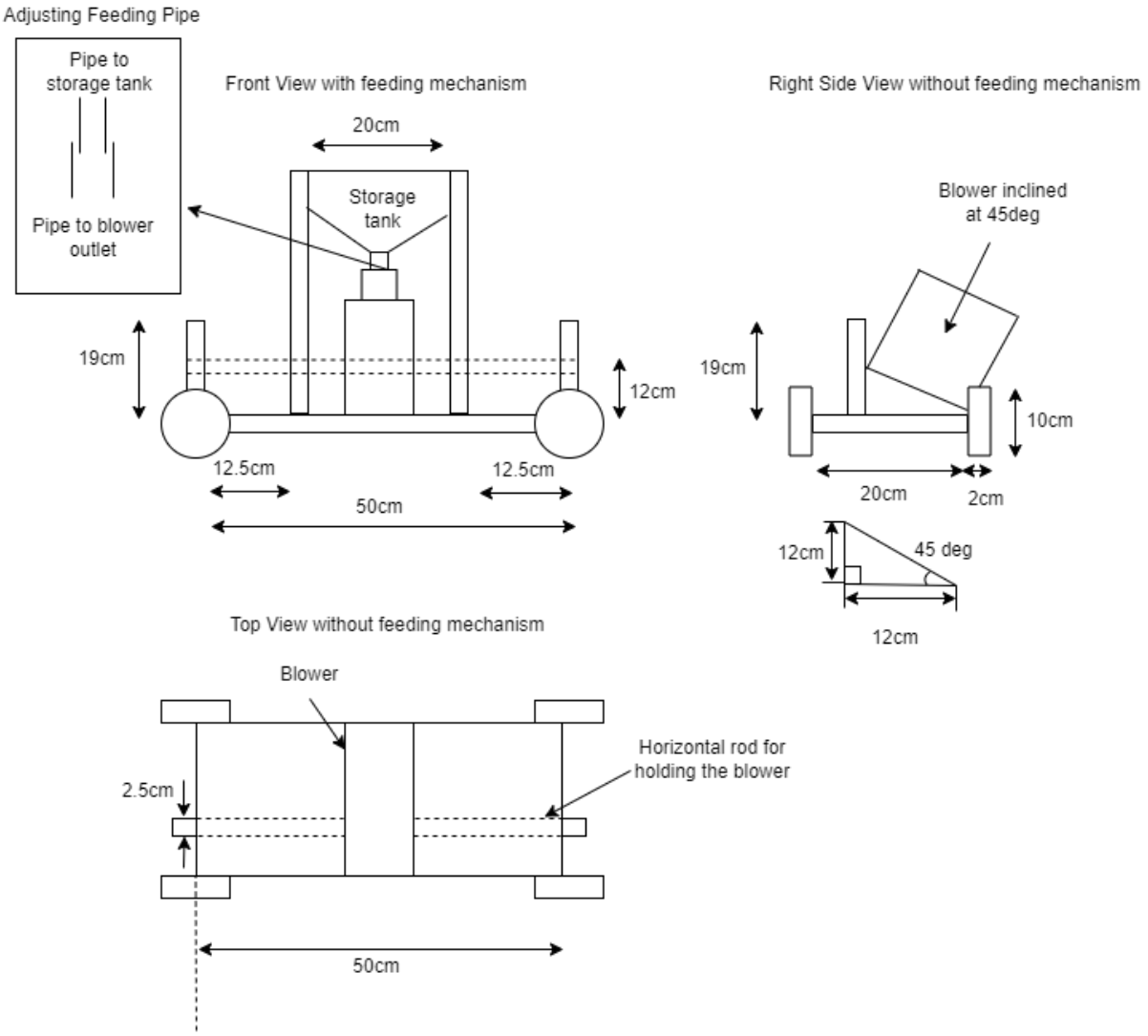

Fig. 4.1. Schematic of the prototype chassis

The total weight of the robot including the blower, channels used for the chassis, feeding mechanism and other components is 6.2 kg. To calculate the torque of the motor, the worst case scenario the robot can be in is considered. That is, it is assumed that the robot is on a slope. The slope that the robot can climb upto was decided to be $\alpha = 30$ degrees.

The robot should move slowly so as to drop the ember particles on every part of the house. It is assumed that the speed of the robot is $v = 0.01$ m/s (1 cm/s). And, the robot should achieve

this speed in 1 s which defines the acceleration as $a = 0.01$ m/s^2. From [37], the total force(F) needed to overcome gravity ignoring friction is given by (4.1),

$$F = m*a + m*g*\sin(\alpha) \ldots(\text{N}) \quad (4.1)$$

where m is the total mass of the robot and g is acceleration due to gravity.

In this report, the force due to friction is also considered to calculate the total force. The coefficient of friction μ for vex wheels made of hard plastic on dry concrete floor is assumed to be 0.3 [38] and is given by,

$$F = m*a + m*g*\sin(\alpha) + \mu*m*g*\cos(\alpha) \ldots(\text{N}) \quad (4.2)$$

$$= (6.2)(0.01) + (6.2)(9.81)\sin(30) + (0.3)(6.2)(9.81)(0.86) = 46.16 \text{ N}$$

The required total torque (T) of four motors that can drive the chassis can be calculated as

$$T = r*F \ldots(\text{N-m}) \quad (4.2)$$

$$= 0.05 \text{ x } 46.16 = 2.30 \text{ N-m.}$$

That is, each motor needs a torque of $T/4 = 0.57$ N-m.

The mechanical power needed for the motors to carry the robot is given by(4.3),

$$P = F*v \ldots(\text{W}) \quad (4.3)$$

$$= 46.16 \text{ x } 0.01 = 0.46 \text{ W.}$$

In this prototype, the Vex 393 DC motors are used from the vex kit. Out of the four motors used, two motors with an integrated encoder module are used. One encoder motor is mounted on each side of the robot. The encoders are used to keep track of the position of the robot. Also, the encoded motors used on each side will help drive the robot in a straight line. This can be achieved by implementing a control algorithm. The specifications of the vex DC motors are shown in the Table 4.1. below. The vex 393 motors are rated for 7.2 V with a stall torque of 1.67 N-m and a stall current of 4.8 A.

The angular speed (ω) of the 0.1 m wheels when connected to the motors is,

$$\omega = 2*pi*(RPM)/60 = 10.47\text{rad/s} \quad (4.4)$$

So, the velocity of the robot would be,

$v = r*\omega$ (4.5)

$= 0.05 \times 10.47 = 0.52$ m/s.

It is clear that the motors cannot be used as is since the robot would move quickly and would not shower the ember simulant thoroughly on the house. To decrease the speed of the robot gears were used. The setup shown in Fig. 4.2. was used to decrease the speed which uses a 12 teeth gear linked to a 60 teeth gear and another 12 teeth gear linked to a 84 teeth gear. The resulting gear ratio then becomes,

Gear ratio = (60/12) * (84/12) = 35:1 (4.6)

As a result, the speed is reduced to around 3 rpm, i.e, around 0.015 m/s which is desirable. The encoder produces a reading of around 95/rotation of the wheel. That is, for

Circumference of the wheel = 2*pi*0.05 = 0.314m (4.7)

The encoder produces 95 readings per rotation of the wheel. So to travel 0.91m(3ft) distance, which is the width of the house, the motors should run till the encoder count is 277.

Table 4.1. Specifications of Vex 393 Motors*

Rated Voltage	7.2 V
Stall Current	4.8 A
Stall Torque	1.67 N-m
Free Speed	100 RPM
Free Current	0.37 A

*Note: Datasheet of Vex 393 can be found in Appendix A.

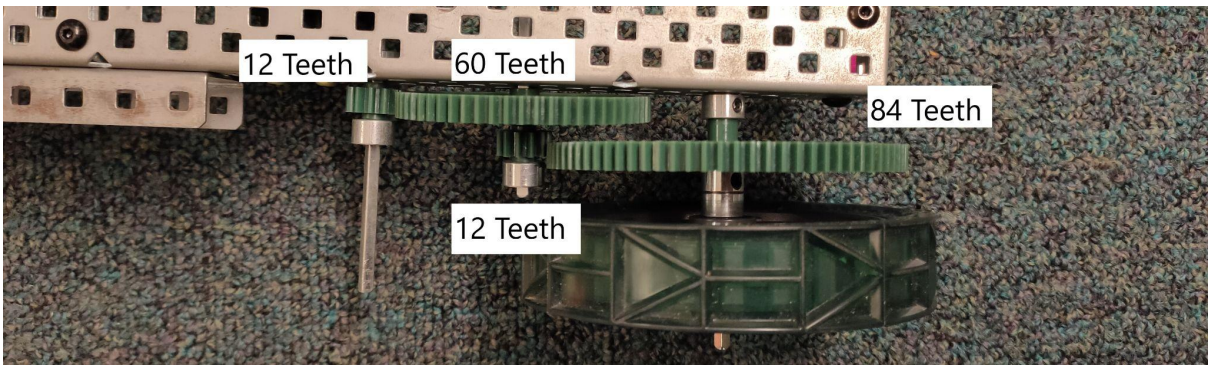

Fig. 4.2. Gear arrangement of the chassis

This gear arrangement was done for all four chassis motors. Fig. 4.3, shows an image of the front, side and top view of the lab-scale ember simulator prototype without the feeding mechanism.

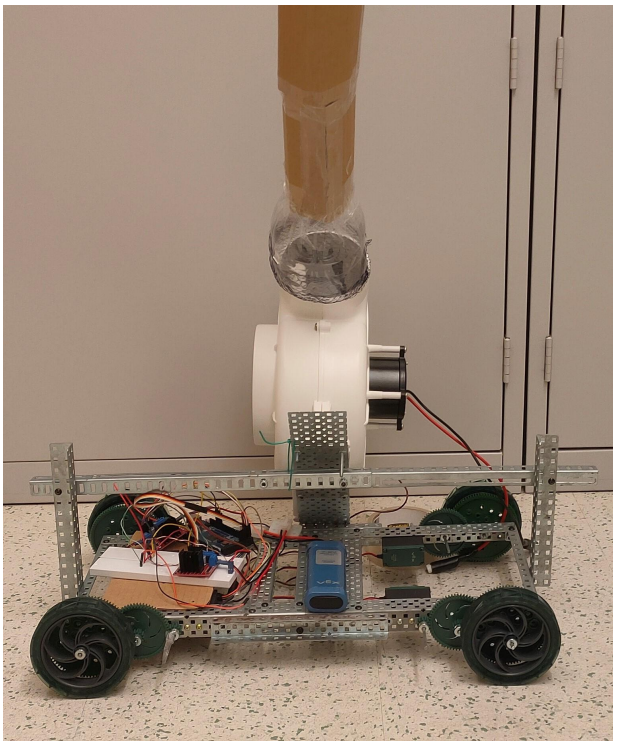

Fig. 4.3 (a). Front view of the lab-scale ember simulator prototype

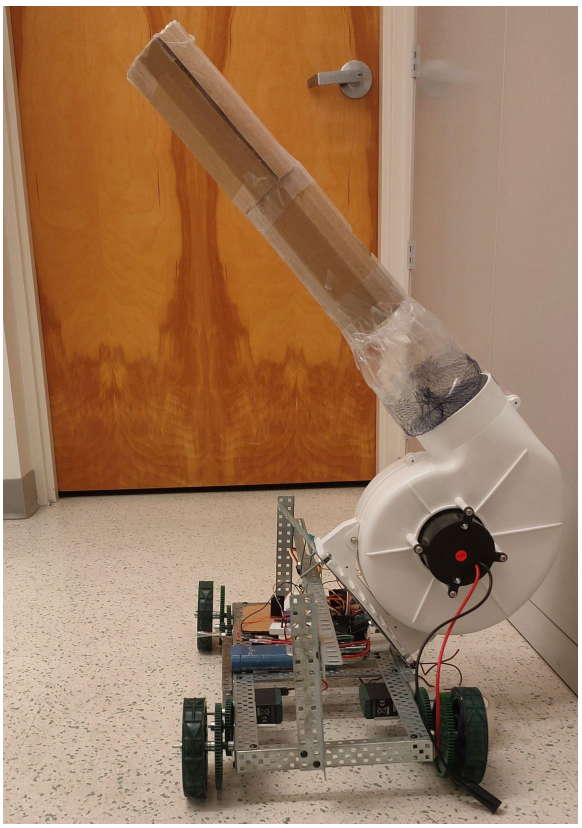

Fig. 4.3 (b). Side view of the lab-scale simulator prototype

Fig. 4.3 (c). Top view of the lab-scale ember simulator prototype

4.3 Motor Driver

These motors were controlled by the Arduino Mega 2560 microcontroller via the L298N motor drivers. A motor driver is a current amplifier that converts low-current signals from the microcontroller to a proportionally higher current that drives the motor. It can also be used to control the direction in which a motor rotates. This is achieved by an H-bridge circuit as shown in Fig. 4.4. An H-bridge circuit is a simple circuit that allows the load, in this case a motor, to run in clockwise or anti-clockwise direction based on the switches turned-on. As shown in Fig. 4.4., the H-bridge comprises four NPN transistors with four diodes for reverse protection. When Q1 and Q4 are turned on while Q2 and Q3 are turned off, +Vcc is connected to motor terminal A and GND is connected to motor terminal B which causes the motor to rotate in one direction. And, when Q2 and Q3 are turned on while Q1 and Q4 are off, the motor terminals A and B are connected to GND and +Vcc respectively, which rotates the motor in the opposite direction. An L298N motor driver is capable of driving two motors.

For controlling four motors two drivers were used. The pinout diagram and specifications of the motor driver are shown in Table 4.2. and Table 4.3. respectively.

Table 4.2. Pinout of L298N**

Pin Name	Description
IN1 & IN2	Control direction of motor A
IN3 & IN4	Control direction of motor B
ENA	Enables PWM signal for Motor A
ENB	Enables PWM signal for Motor B
OUT 1 & OUT 2	Output Pins of Motor A
OUT 3 & OUT 4	Output Pins of Motor B
12 V	Input Voltage to the Chassis Motors
5 V	Power supply for logic switching in L298N
GND	Ground Pin

Table 4.3. Specifications of L298N** Motor Driver.

Parameter	Rating
Driver Voltage	5-35 V
Driver Current	2 A
Logic Voltage	5 V
Logic Current	0-36 mA
Maximum Power	25 W

**Note: Datasheet of motor driver L298N can be found in Appendix B.

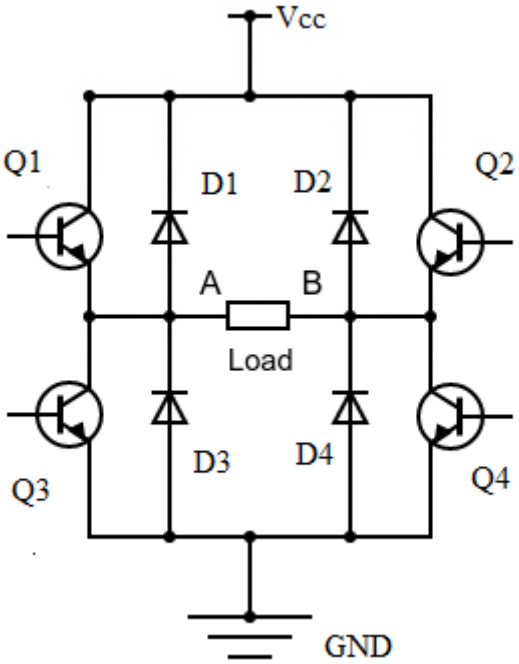

Fig. 4.4. Basic H-bridge

As shown in the pinout, a motor can be controlled from three pins by the microcontroller. Two pins INx (x = 1 or 3) and INy (y = 2 or 4) control the direction in which the motor rotates. For example, if a motor is connected on PORT 1 of the motor controller, it rotates in clockwise direction when IN1 = HIGH and IN2 = LOW. When IN1 = LOW and IN2 = HIGH, then the motor will rotate anti-clockwise. To control the speed at which a motor rotates, the ENx pin can be used. When the ENz (z = A or B) pin is shorted with a jumper on the motor controller, the motor runs at full speed. When not shorted, this pin can be connected to a PWM pin of the arduino mega microcontroller and the speed of the motor can be controlled by passing a pulse width modulated signal from the microcontroller.

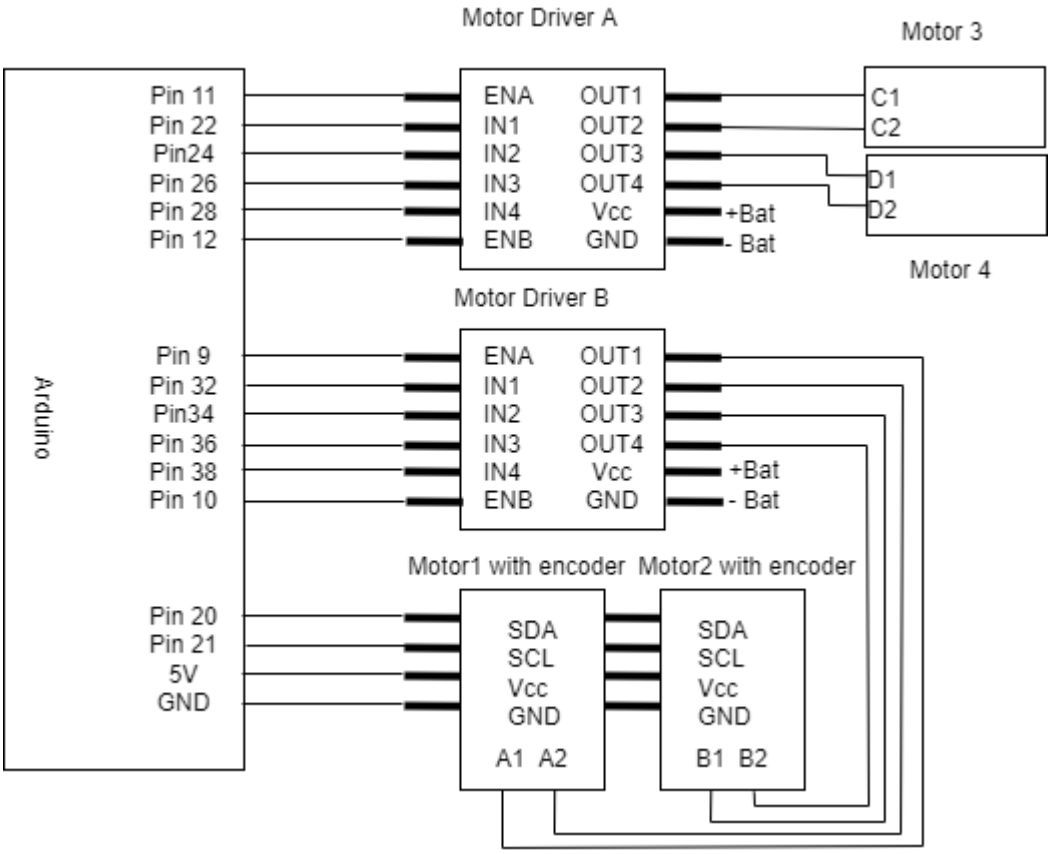

Fig 4.5. Motor connections to the microcontroller

4.4 Microcontroller

To control the chassis, an arduino mega microcontroller is used. Arduino is an open-source electronics platform that can be used to interface components easily and code them using the open source Arduino software called the Arduino Integrated Development Environment (IDE). The arduino mega has an atmega2560 chip with 54 digital input/output pins out of which 13 pins can be used to generate PWM signals, four ports or 8 pins for (Universal Asynchronous Receiver Transmitter) UART communication, SDA and SCL pins for I2C (Inter Integrated Circuit Communication) and MISO, MOSI pins for SPI (Serial Peripheral Interface) communication. Additionally, it is also capable of reading analog

signals and has 16 pins dedicated to do that. The microcontroller works on a 16 MHz crystal oscillator and can be powered using a power jack and a USB connection on board [39].

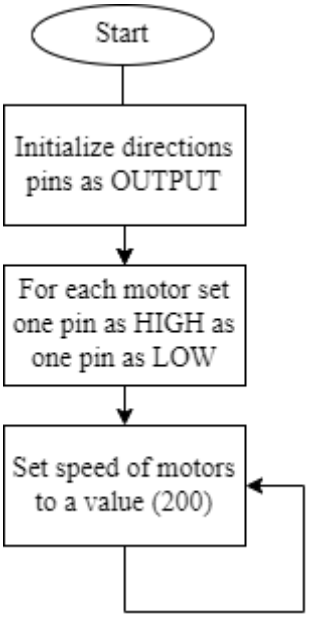

Fig. 4.6. Flowchart of code with no feedback.

The arduino microcontroller in this project is used to control the motors and read inputs from the switches to start and stop the chassis. The motors were connected to the microcontroller as shown in Fig. 4.5. and the code as shown in flowchart Fig. 4.6. was uploaded to the arduino board. In Fig. 4.5., A1, A2, B1, B2, C1, C2, and D1, D2 are motor terminals. As expected with no feedback in this control system, the chassis did not move in a straight line. The results are discussed later in this chapter. The blower is expected to shower the ember materials through the whole width of the house. With no feedback system, it failed to do so and deviated from its course. To correct this, a sensor can be added which will provide necessary feedback to the microcontroller about the robot's position. For this, two motors with an integrated encoder module were used. On rotation, the encoder module will produce pulses which will be read by the arduino. It will then supply the speed signals according to the encoder readings. The encoders are connected to the arduino on the I2C port, i.e, the SDA (Serial Data) and SCL (Serial Clock) pins.

4.5 Inter-Integrated Circuit (I2C) Communication

I2C is a serial communication protocol where the data is transferred bit by bit along a single wire, the Serial Data (SDA) line. It is a synchronized form of communication where the data transfer is sampled by the Serial clock (SCL) signal shared by the master and slave device. This clock signal is controlled by the master device. The data in this form of communication is transferred in messages which are broken in frames of data. A message is represented as shown in Fig. 4.7. by frames like: Start bit, an address frame of 7 or 10 bits, Read/Write bit, Acknowledgement/No-Acknowledgement bit between each Data frame of 8 bits and finally the stop bit [40].

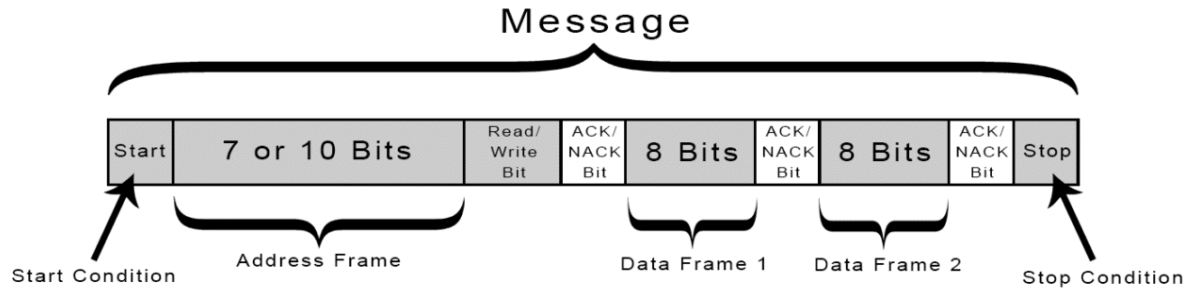

Fig. 4.7. I2C Message Transfer [40]

The start and stop bits as the name suggests denotes the start and end of the protocol. The address is a 7 or 10 bit unique sequence given to each slave device in order to communicate to that device. To specify whether the master is reading or writing from the slave device, the read/write bit is used. In I2C communication, at a time 8 bits of data can be transferred. After the address and the data frames the acknowledgment/no-acknowledgment bit (ACK/NACK) bit denotes whether the transfer of these frames was successful or not. After the acknowledgement bit is successfully received the next data frame can be transferred

in the same message. After all the data frames have been sent, the stop bit is sent to the slave device to halt the transmission of data.

It is an effective form of communication with only two wires. The integrated encoder module in the motor communicates with the arduino using the I2C communication protocol. The encoder module of the second motor is daisy chained to the microcontroller through the other motor. The encoder readings are used to drive the chassis carrying the blower in a straight line.

Fig. 4.8 (a). shows the encoder readings (scaled value of ticks) of both the motors which shows the gap between the two readings is increasing. This gap is the error shown in Fig. 4.8 (b). This error is the difference between the two encoder modules of the motors. The error can be a result of a number of reasons like uneven surface, which may cause the wheel to not be in proper contact with the ground; motors not performing in an identical manner; the weight of mechanisms on the chassis could be loaded on one side of the robot which could also be a cause for the error. Initially, the encoder modules were just used to take readings and no feedback loop was implemented. As it can be seen from Fig. 4.8 (b)., the error is growing continuously when the robot was run for a total distance of three feet. To reduce this error, it is important to implement a control algorithm.

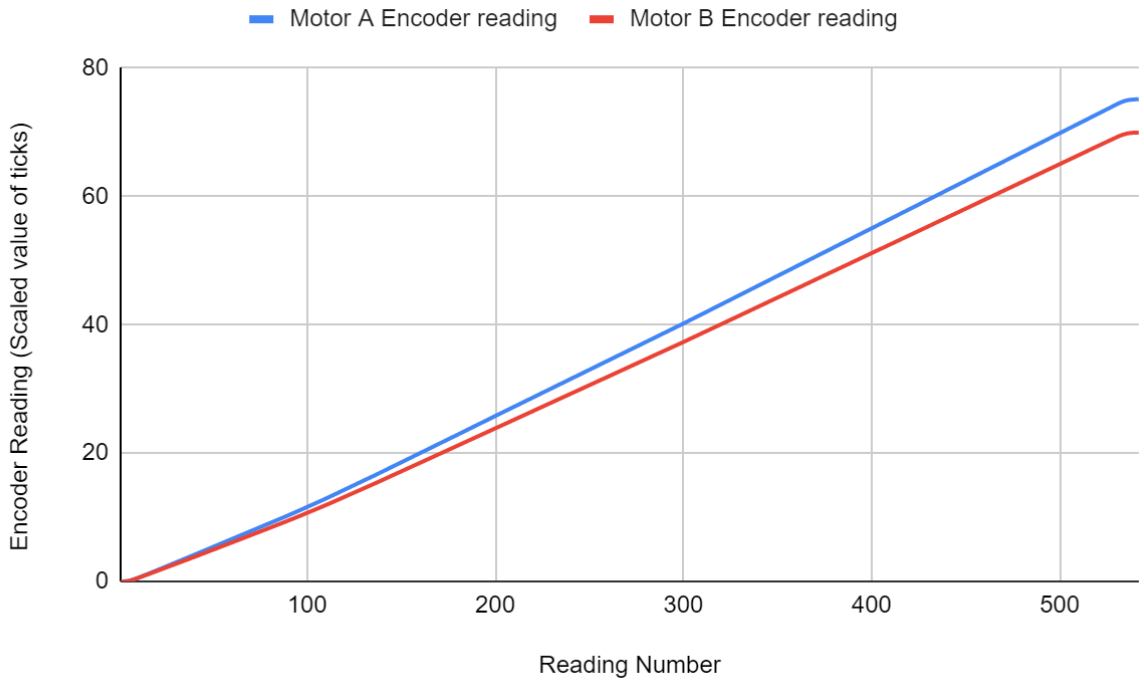

Fig. 4.8 (a). Encoder Readings of both the motors with no control algorithm

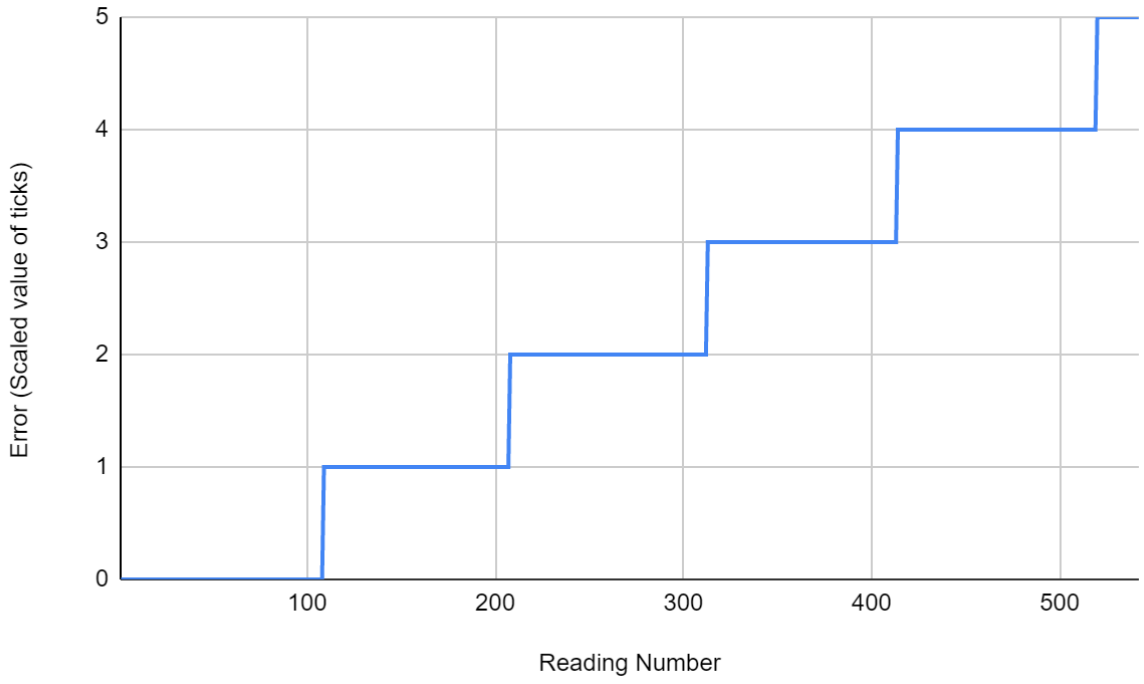

Fig. 4.8 (b). Calculated Error with no control algorithm

4.6 Implementing the Proportional Control Algorithm

The encoded motors are used on each side of the chassis. So when the chassis is driven the motors produce readings for each side. The input from the encoders are read from the I2CEncoder library [41] and the wire library provided by Arduino for I2C communication. After declaring the motor control pins as output pins the motors are initially run on constant speed and the readings from the encoder are read by the microcontroller. In order to move in a straight line, the readings from both the encoders should be the same. This is the main idea of applying any control algorithm. If the robot deviates from its path, the encoder readings of the motor will differ. The difference between the readings is called the error. This error can be removed by giving speed signals proportional to error. To minimize this error, the speed of motor A is decreased by some value and the speed of motor B will be increased by the same value. In this case, the error can be positive or negative, i.e., if the encoder readings of motor A are greater than motor B then the error will be positive else it will be negative. Depending on the error produced, it is scaled to generate a value by the proportional constant, *Kp*. Hence, the speed of motor B will be increased proportionally by *Kp*error* and the speed of motor A will be decreased by the same value. The constant Kp in this experiment was found by trial-error method. It was found that $Kp = 5$ produced desirable results which is discussed below. The implementation of this algorithm is shown by the flowchart Fig. 4.9.

The results are attached below in Fig. 4.10 (a). and Fig. 4.10 (b). Fig. 4.10 (a). shows 435 samples of the motor encoder readings (scaled value of ticks). The difference between the speed can be seen decreasing after around 375 samples where the error too can be seen oscillating between 3 and 4 in Fig. 4.10 (b). This decrease in difference is because of the

change in the speed proportional to the error produced. This decrease in error causes the robot to move in a straight line.

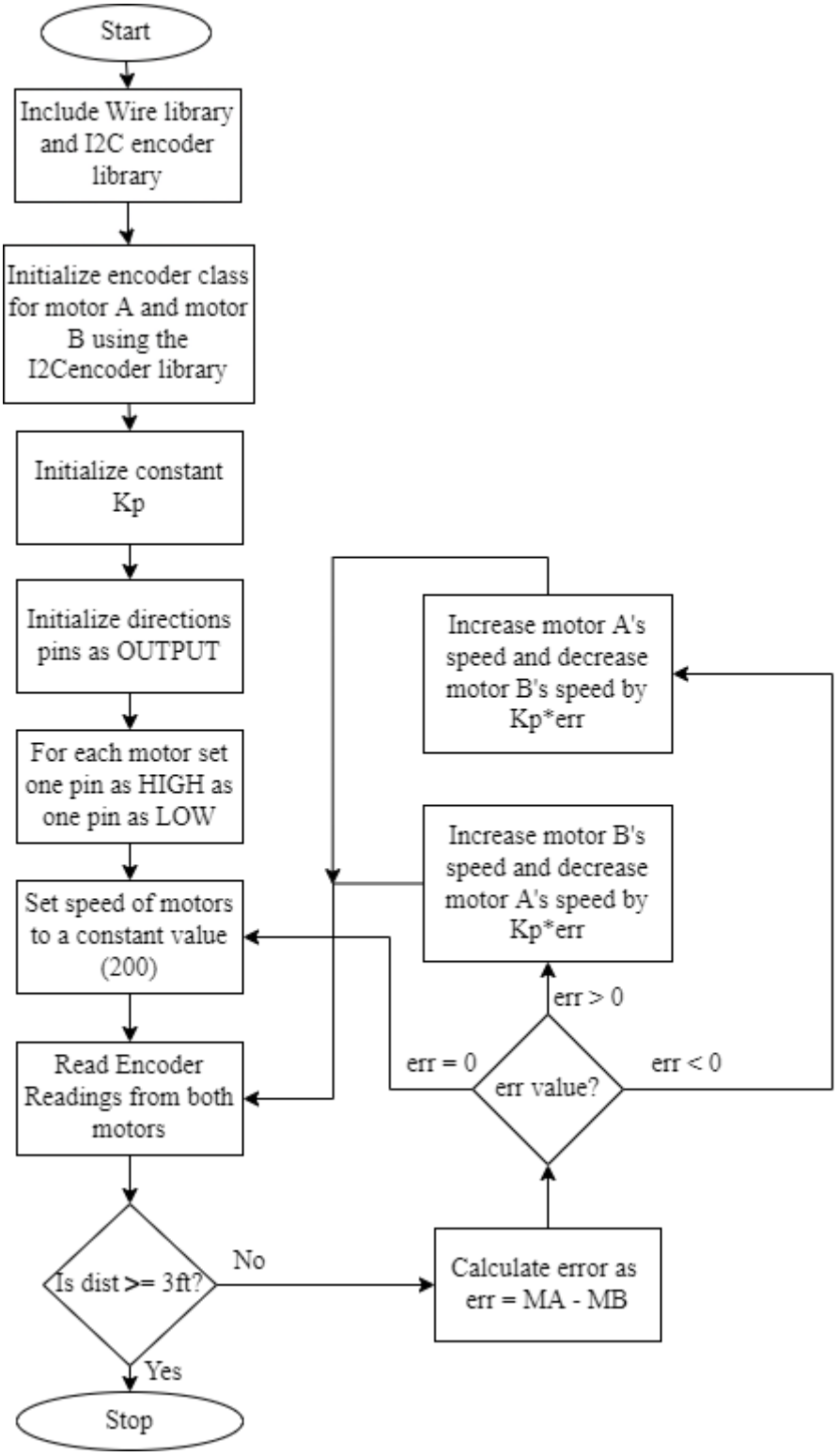

Fig. 4.9. Flowchart of code with Proportional Control algorithm

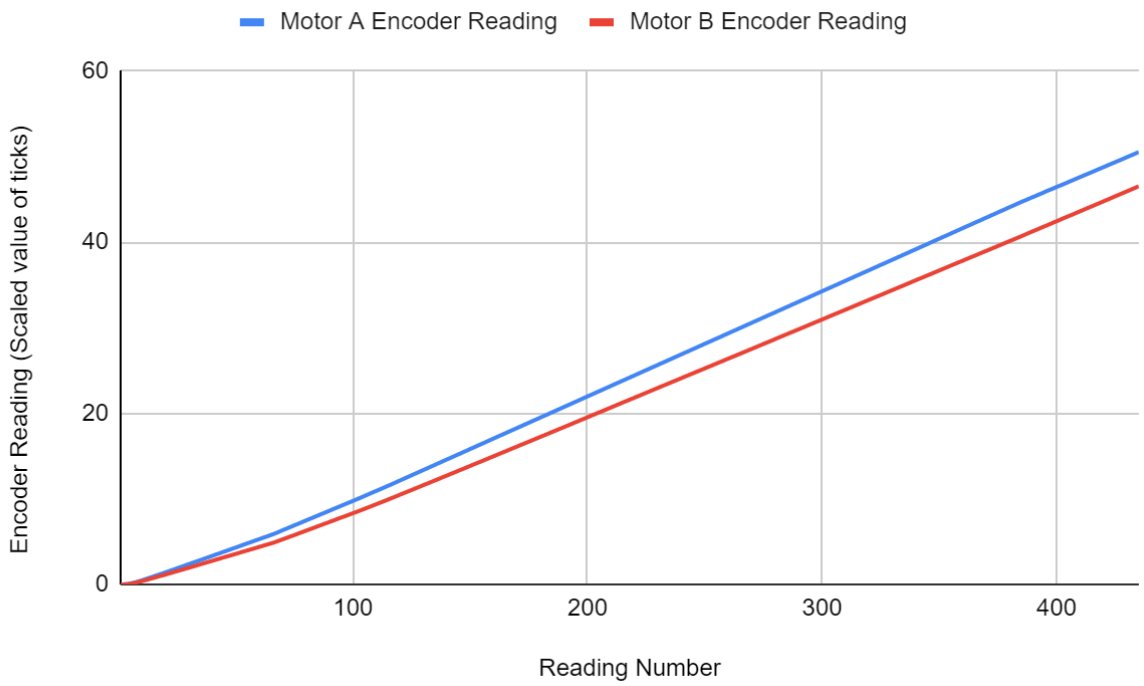

Fig. 4.10 (a). Encoder Readings from the two motors

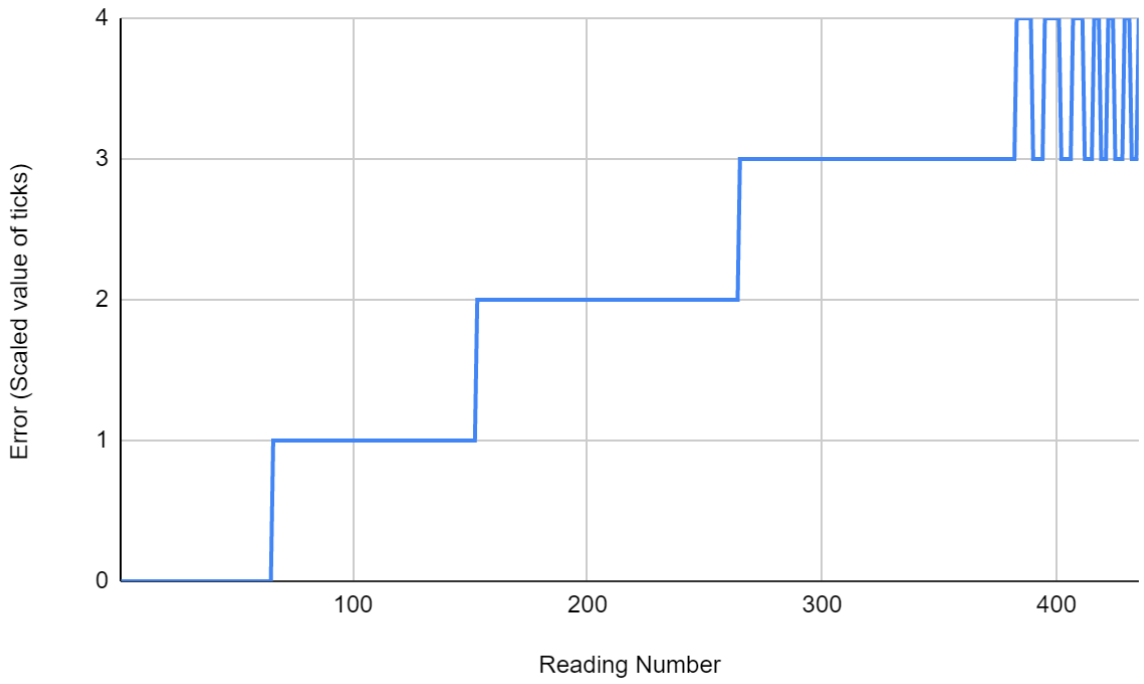

Fig. 4.10 (b). Integer Error value over 435 samples

Chapter 5

Conclusions

5.1 Summary of the work done

In this report, a prototype of an ember simulator is discussed. This prototype is capable of projecting ember simulants onto a model house of height 6 ft and 3 ft wide when placed 6 ft away. The ember simulant selected is non-flammable, biodegradable and can be collected using a vacuum cleaner. All conditions set by FireSmart for the selection of fake ember material are met by using c;oth balls. These balls are available in variable sizes similar to actual embers which helps make the simulation close to the actual forest fires. A centrifugal blower was used to project these ember materials. The selected centrifugal blower with four inch outlet and 440 CFM was able to propel the ember material on the model house. The feeding mechanism designed could feed the embers to the blower outlet. The angle of the blower mechanism can be changed manually and the same structure of the feeding mechanism can be used when the blower is inclined at different angles. This apparatus is mounted on a rectangular chassis which is run by four DC motors out of which two have encoded motors. The motors were controlled by the arduino microcontroller through the L298N motor driver. The readings of the encoded motors are read by the arduino microcontroller using I2C communication. To ensure the motors move in a straight line, a proportional control algorithm was applied. The difference in the encoder readings produced an error and the speed of the motors were controlled by passing signals proportional to the error produced. As a result, the robot was able to project ember material on the wall of the model house of height 6 ft and width 3 ft and was driven 6 ft apart from the house. The robot was able to drive itself along a straight line.

5.2 Future Scope

Although the selected ember material meets all conditions set by FireSmart a potential issue related to collecting the ember materials is predicted. When the ember materials are projected on a real house, the surroundings of the house will have leaves, dust, pebbles of weight and dimensions similar to the embers. These materials will also be sucked by the vacuum cleaner and for the next use, this batch of ember materials should be segregated before using in order to avoid damage to the house to be tested.

In the designed prototype, only one blower is used to project the ember materials on the house. There can be multiple setups like the one discussed in this report used simultaneously to project ember materials on a house. Moreover, to increase the range of the ember materials projected, two blowers can be connected such that they have one output. This experiment can help in increasing the range and height of the projectile of the ember materials and reduce the cost of expensive high CFM blowers.

The prototype reported in this work was experimented in a laboratory. The projectile followed by a projected ember simulant was not affected by the external environment. But in real life weather can have a significant effect on the trajectory of the light ember materials. In the best case scenario, the direction of the wind can be in the same direction of the ember that is being projected. But, the direction of wind different than that will account as a worst case scenario, which could cause the embers to completely miss the target house. To solve this problem, high CFM blowers can be used and the trajectory of few ember materials can be tested.

Bibliography

1. National Geographic Society, “Wildfires,” *National Geographic Society*, 15-Jul-2019. [Online]. Available: https://www.nationalgeographic.org/encyclopedia/wildfires/. [Accessed: 12-Apr-2022].
2. Chelene C. Hanes, Xianli Wang, Piyush Jain, Marc-André Parisien, John M. Little, and Mike D. Flannigan. Fire-regime changes in Canada over the last half century. Canadian Journal of Forest Research. 49(3): 256-269. https://doi.org/10.1139/cjfr-2018-0293
3. Stocks, B.J., Mason, J.A., Todd, J.B., Bosch, E.M., Wotton, B.M., Amiro, B.D., Flannigan, M.D., Hirsch, K.G., Logan, K.A., Martell, D.L., Skinner, W.R., 2002. Large forest fires in Canada, 1959–1997. Journal of Geophysical Research: Atmospheres 107 (D1), FFR 5–1–FFR 5–12.
4. Coogan Sean C. P., Cai Xinli, Jain Piyush, Flannigan Mike D. (2020) Seasonality and trends in human- and lightning-caused wildfires ≥ 2 ha in Canada, 1959–2018. International Journal of Wildland Fire 29, 473-485. https://doi.org/10.1071/WF19129
5. Sean C.P. Coogan, Lori D. Daniels, Den Boychuk, Philip J. Burton, Mike D. Flannigan, Sylvie Gauthier, Victor Kafka, Jane S. Park, and B. Mike Wotton. Fifty years of wildland fire science in Canada. Canadian Journal of Forest Research. 51(2): 283-302. https://doi.org/10.1139/cjfr-2020-0314
6. B. C. W. Service, “Wildfire season summary,” *Province of British Columbia*, 28-Mar-2022. [Online]. Available:

https://www2.gov.bc.ca/gov/content/safety/wildfire-status/about-bcws/wildfire-history/wildfire-season-summary?keyword=wildfire. [Accessed: 12-Apr-2022].

7. Mamuji, A.A., Rozdilsky, J.L. Wildfire as an increasingly common natural disaster facing Canada: understanding the 2016 Fort McMurray wildfire. Nat Hazards 98, 163–180 (2019). https://doi.org/10.1007/s11069-018-3488-4
8. Tymstra, Cordy & Stocks, Brian & Cai, Xinli & Flannigan, Mike. (2019). Wildfire management in Canada: Review, challenges and opportunities. Progress in Disaster Science. 5. 100045. 10.1016/j.pdisas.2019.100045.
9. Filkov, Alexander & Ngo, Tuan & Matthews, Stuart & Telfer, Simeon & Penman, Trent. (2020). Impact of Australia's catastrophic 2019/20 bushfire season on communities and environment. Retrospective analysis and current trends. Journal of Safety Science and Resilience. 1. 10.1016/j.jnlssr.2020.06.009.
10. Brown, T., Leach, S., Wachter, B., & Gardunio, B. (2020). The Extreme 2018 Northern California Fire Season, Bulletin of the American Meteorological Society, 101(1), S1-S4. Retrieved Apr 3, 2022, from https://journals.ametsoc.org/view/journals/bams/101/1/bams-d-19-0275.1.xml
11. D. Jergler, "Burning down a house to show how to build for wildfire defense," *Insurance Journal*, 24-Mar-2019. [Online]. Available: https://www.insurancejournal.com/news/national/2019/03/20/521093.htm. [Accessed: 12-Apr-2022].
12. "Who we are," *FireSmart BC*, 14-Feb-2022. [Online]. Available: https://firesmartbc.ca/who-we-are/. [Accessed: 12-Apr-2022].
13. "Understanding the residential development standards (ResCode)." [Online]. Available:

https://www.planning.vic.gov.au/__data/assets/pdf_file/0030/97158/PPN27-Understanding-the-Residential-Development-Standards-ResCode_June-2015.pdf. [Accessed: 12-Apr-2022].

14. “Planning Schemes.” [Online]. Available: https://www.planning.vic.gov.au/__data/assets/pdf_file/0026/94535/1_Planning-Schemes.pdf. [Accessed: 12-Apr-2022].
15. Foote, Ethan & Liu, John & Manzello, Samuel. (2011). Characterizing firebrand exposure during wildland-urban interface fires. Conference Proceedings - Fire and Materials 2011, 12th International Conference and Exhibition.
16. Rissel, Sean; Ridenour, Karen. 2013. Ember production during the Bastrop Complex Fire. Fire Management Today 72(4):7-13.
17. Filkov, Alexander & Prohanov, Sergey & Mueller, Eric & Kasymov, Denis & Martynov, Pavel & El Houssami, Mohamad & Thomas, Jan & Skowronski, Nicholas & Butler, Bret & Gallagher, Michael & Clark, Kenneth & Mell, William & Kremens, Robert & Hadden, Rory & Simeoni, Albert. (2016). Investigation of firebrand production during prescribed fires conducted in a pine forest. Proceedings of the Combustion Institute. 36. 10.1016/j.proci.2016.06.125.
18. El Houssami, M., Mueller, E., Filkov, A. et al. Experimental Procedures Characterizing Firebrand Generation in Wildland Fires. Fire Technol 52, 731–751 (2016). https://doi.org/10.1007/s10694-015-0492-z
19. Manzello, Samuel & MaranghidesA, Alexander & Mell, William. (2007). Firebrand generation from burning vegetation. Int J Wildland Fire 16: 458-462. International Journal of Wildland Fire - INT J WILDLAND FIRE. 16. 10.1071/WF06079.

20. Manzello, Samuel & Maranghides, Alexander & Shields, John & Mell, William & Hayashi, Yoshihiko & Nii, Daisaku. (2007). Measurement of firebrand production and heat release rate (hrr) from burning Korean pine trees. 7.
21. Manzello SL, Shields JR, Cleary TG, et al. On the development and characterization of a firebrand generator. Fire Safety J 2008; 43: 258–268.
22. Manzello SL, Park S-H, Shields JR, et al. Comparison testing protocol for firebrand penetration through building vents: summary of BRI: NIST full scale and NIST reduced scale results (NIST technical note 1659). Gaithersburg, MD: National Institute of Standard and Technology, 2010.
23. Sharifian, A., & Hashempour, J. (2016). A novel ember shower simulator for assessing performance of low porosity screens at high wind speeds against firebrand attacks. *Journal of Fire Sciences, 34*, 335 - 355.
24. Manzello, Samuel & Park, Seul-Hyun & Suzuki, Sayaka & Shields, John & Hayashi, Yoshihiko. (2011). Experimental investigation of structure vulnerabilities to firebrand showers. Lancet. 46. 568-578. 10.1016/j.firesaf.2011.09.003.
25. Sharifian A and Buttsworth D. Double-layered metal mesh screens to contain or exclude thermal radiation from bush fires. J Fire Prot Eng 2010; 20(4): 291–311.
26. Pagonis, V. & Guerra, David & Chauduri, Sean & Hornbecker, Brian & Smith, Nathan. (1997). Effects of air resistance. The Physics Teacher. 35. 364-368. 10.1119/1.2344721.
27. Parker, G.. (1977). Projectile motion with air resistance quadratic in the speed. American Journal of Physics - AMER J PHYS. 45. 10.1119/1.10812.
28. Cross, Rod. (2012). Measuring the Effects of Lift and Drag on Projectile Motion. The Physics Teacher. 50. 80-82. 10.1119/1.3677279.

29. Sarafian, H. (2015) Impact of the Drag Force and the Magnus Effect on the Trajectory of a Baseball. World Journal of Mechanics, 5, 49-58. doi: 10.4236/wjm.2015.54006.
30. Pantaleone, J. & Messer, J.. (2011). The added mass of a spherical projectile. American Journal of Physics. 79. 1202-1210. 10.1119/1.3644334.
31. Chudinov, Peter. (2014). Approximate Analytical Description of the Projectile Motion with a Quadratic Drag Force. ATHENS JOURNAL OF SCIENCES. 1. 97-106. 10.30958/ajs.1-2-2.
32. J. Yu, T. Zhang, and J. Qian, "Classification: electric motors, pumps, fans," in *Electrical Motor Products: International energy -efficiency standards and testing methods*, WOODHEAD, 2016.
33. A. Bailes, "What happens to air flow in ducts when size changes?," *Energy Vanguard*, 29-Oct-2018. [Online]. Available: https://www.energyvanguard.com/blog/what-happens-air-flow-ducts-when-size-changes/. [Accessed: 12-Apr-2022].
34. "AirV - radial blowers," *SPX FLOW*. [Online]. Available: https://www.spxflow.com/johnson-pump-marine/products/airv-radial-blowers/. [Accessed: 12-Apr-2022].
35. "IBHS research center ember storm test highlights - youtube," *YouTube*, 25-Apr-2011. [Online]. Available: https://www.youtube.com/watch?v=IvbNOPSYyss. [Accessed: 13-Apr-2022].
36. "VEX cortex starter kit," *Cortex Classroom Starter Kit - VEX Robotics*. [Online]. Available: https://www.vexrobotics.com/276-7510.html#attr-vex_kit_contents. [Accessed: 12-Apr-2022].
37. A. J. Neal, "Tips For Selecting DC Motors For Your Mobile Robot," *SERVO Magazine* , Jan-2010.

38. “Friction coefficients between different wheel/tire materials and concrete,” *EML2322L -- friction coefficients*. [Online]. Available: https://mae.ufl.edu/designlab/Class%20Projects/Background%20Information/Friction%20coefficients.htm. [Accessed: 14-Apr-2022].
39. Atmel, “Atmel ATmega640/V-1280/V-1281/V-2560/V-2561/V,” ATMega2560 datasheet, Feb. 2014.
40. S. Campbell, “Basics of the I2C communication protocol,” *Circuit Basics*, 14-Nov-2021. [Online]. Available: https://www.circuitbasics.com/basics-of-the-i2c-communication-protocol/. [Accessed: 12-Apr-2022].
41. A. Henning, “Alexhenning/i2cencoder: Arduino library to interface with the VEX integrated encoders using I2C.,” *GitHub*, 19-Jul-2018. [Online]. Available: https://github.com/alexhenning/I2CEncoder. [Accessed: 12-Apr-2022].

Appendix A

Datasheet of Vex 393 Motor

Motion Accessories

2 Wire Motor 393

The 2 Wire Motor 393 provides up to 60% more torque than the standard motor, which will allow more powerful mechanisms and drive bases. All of the internal gears are made from a steel alloy, which means that clutches and replacement gears are no longer required. The 2 wire motor can be directly connected to the Cortex and ARM 9 microcontrollers' internal motor controllers. An external motor control module is required to connect the 2 wire motor to the PIC Microcontroller V0.5. External motor control modules can also be used with the Cortex and ARM 9 microcontrollers.

INSERT THIS PAGE at the **back of the Motion Chapter** in your VEX Inventor's Guide.

High Speed Option

Want to go faster than the standard motor but still have the same output torque as the standard motor? No problem! The 2 Wire Motor 393 kit can be configured into a "high speed" version. Simply follow the "Gear Change Procedure" step-by-step instructions to increase the output speed by 60%.

Motor Coupler

The 2 Wire Motor 393 Kit includes the new shaft coupler which can be used in place of the clutch to connect the motor to VEX shafts. The coupler can also be used to connect VEX shafts together.

Motor Specifications

All motor specifications are at 7.2 volts. Actual motor specifications are within 20% of the values below.

Description	As Shipped	High Speed Option
Stall Torque	13.5 in-lb [1.68 N-m]	8.4 in-lb [1.05 N-m]
Free Speed	100 RPM	160 RPM
Stall Current	3.6 Amps	
Free Current	0.15 Amps	

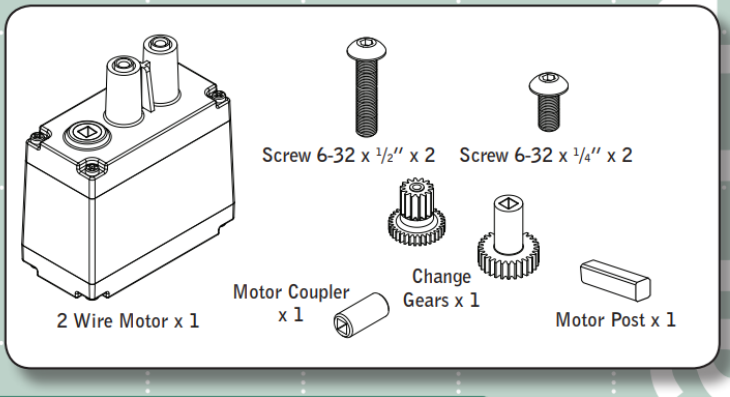

Limited 90-day Warranty
This product is warranted by Innovation First against manufacturing defects in material and workmanship under normal use for ninety (90) days from the date of purchase from authorized Innovation First dealers. For complete warranty details and exclusions, check with your dealer.

Innovation First, Inc.
1519 IH 30 W
Greenville, TX 75402

12/10

For More Information, and additional Parts & Pieces refer to:
www.VEXrobotics.com

2 Wire Motor Kit, continued

Gear Change Procedure

To configure the high speed option, follow these instructions:

1. Remove the four screws in the corners of the front of the motor case.

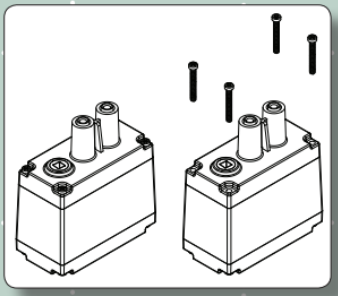

2. Lift off the top cover. Do not disturb the gears inside.

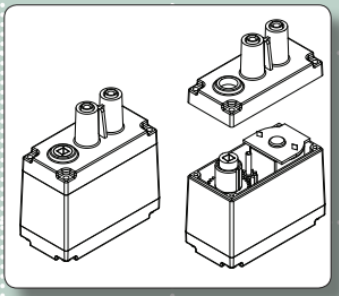

3. Lift off the output bushing and place to the side. This will be used later.

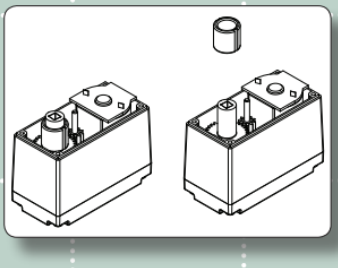

4. Remove the middle gear and the output shaft gear.

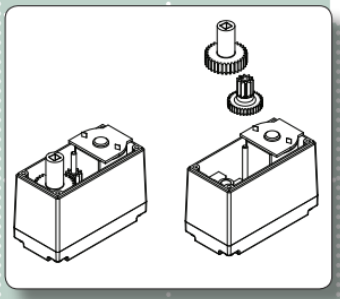

5. Install the high speed middle gear.

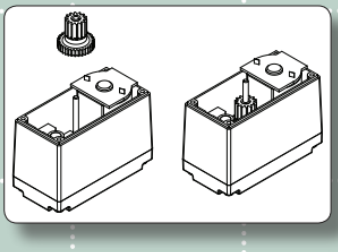

6. Install the high speed output shaft gear.

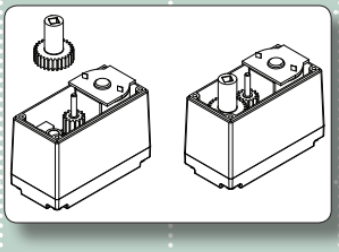

7. Install the output bushing removed in step 3. Make sure the bushing orientation is as shown.

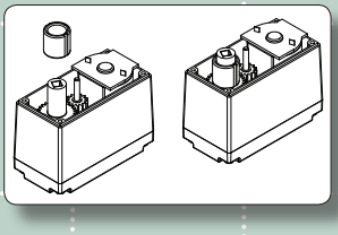

8. Replace the cover and four screws removed in steps 1 and 2.

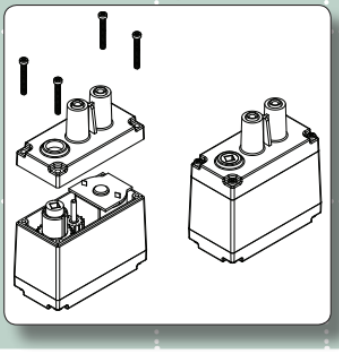

accessories

Appendix B

Datasheet of L298N Motor Driver

L298

DUAL FULL-BRIDGE DRIVER

- OPERATING SUPPLY VOLTAGE UP TO 46 V
- TOTAL DC CURRENT UP TO 4 A
- LOW SATURATION VOLTAGE
- OVERTEMPERATURE PROTECTION
- LOGICAL "0" INPUT VOLTAGE UP TO 1.5 V (HIGH NOISE IMMUNITY)

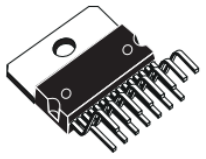

Multiwatt15

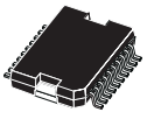

PowerSO20

ORDERING NUMBERS : L298N (Multiwatt Vert.)
L298HN (Multiwatt Horiz.)
L298P (PowerSO20)

DESCRIPTION

The L298 is an integrated monolithic circuit in a 15-lead Multiwatt and PowerSO20 packages. It is a high voltage, high current dual full-bridge driver designed to accept standard TTL logic levels and drive inductive loads such as relays, solenoids, DC and stepping motors. Two enable inputs are provided to enable or disable the device independently of the input signals. The emitters of the lower transistors of each bridge are connected together and the corresponding external terminal can be used for the connection of an external sensing resistor. An additional supply input is provided so that the logic works at a lower voltage.

BLOCK DIAGRAM

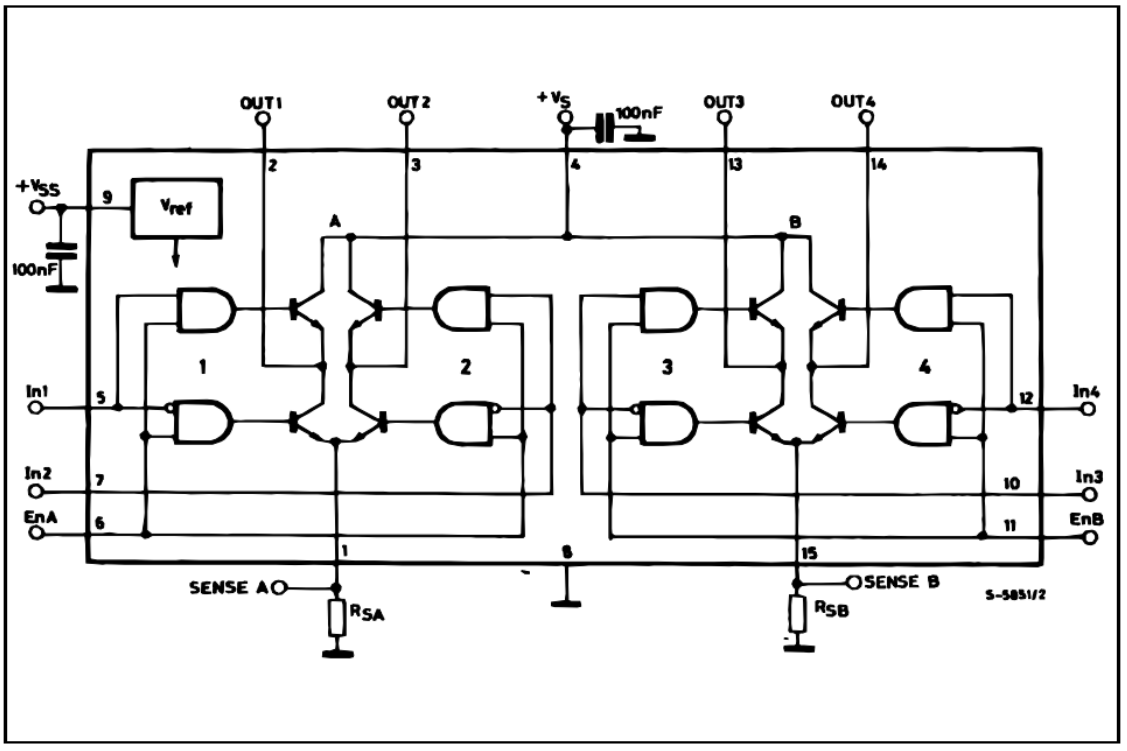

ABSOLUTE MAXIMUM RATINGS

Symbol	Parameter	Value	Unit
V_S	Power Supply	50	V
V_{SS}	Logic Supply Voltage	7	V
V_I,V_{en}	Input and Enable Voltage	–0.3 to 7	V
I_O	Peak Output Current (each Channel) – Non Repetitive (t = 100µs) –Repetitive (80% on –20% off; t_{on} = 10ms) –DC Operation	 3 2.5 2	 A A A
V_{sens}	Sensing Voltage	–1 to 2.3	V
P_{tot}	Total Power Dissipation (T_{case} = 75°C)	25	W
T_{op}	Junction Operating Temperature	–25 to 130	°C
T_{stg}, T_j	Storage and Junction Temperature	–40 to 150	°C

PIN CONNECTIONS (top view)

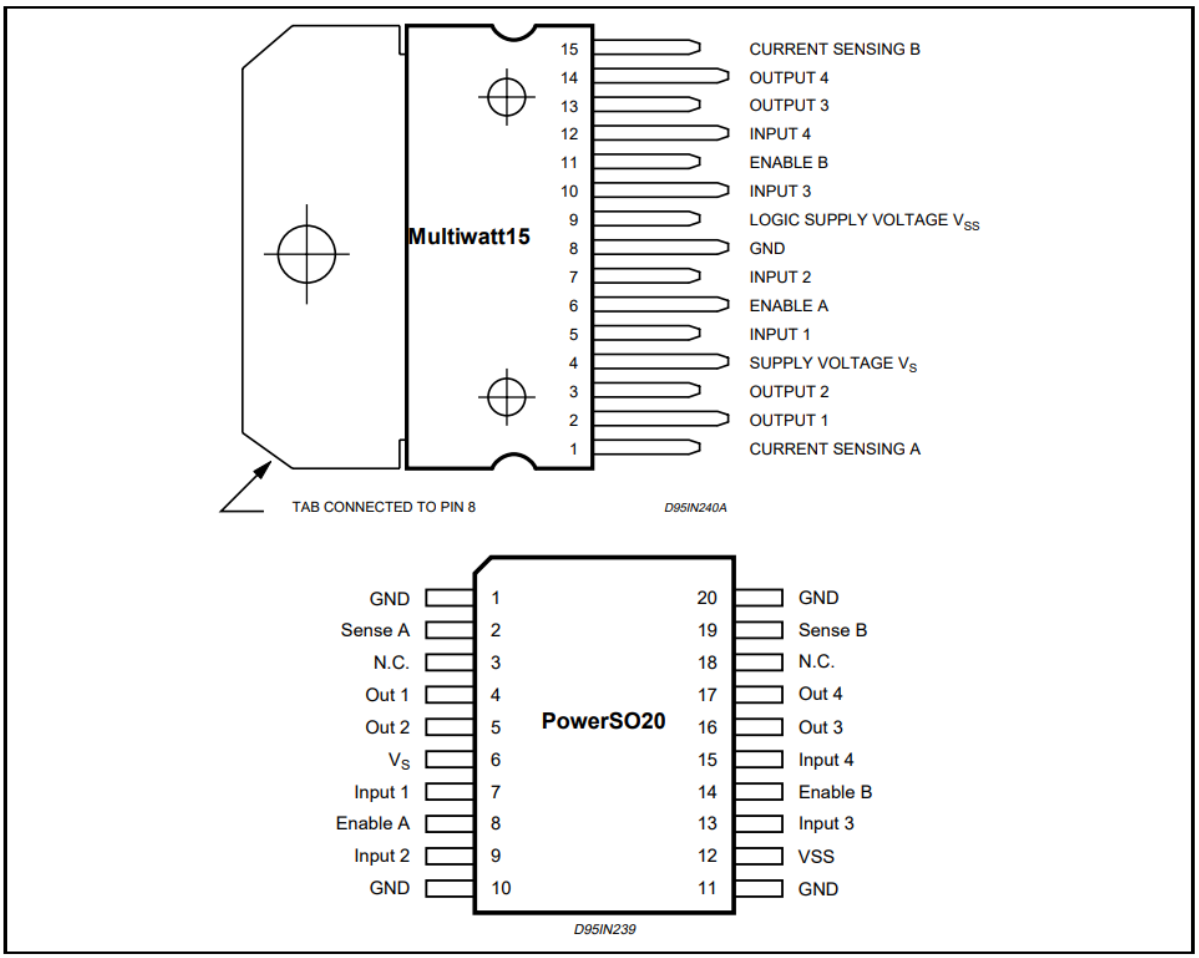

THERMAL DATA

Symbol	Parameter		PowerSO20	Multiwatt15	Unit
$R_{th\ j\text{-}case}$	Thermal Resistance Junction-case	Max.	–	3	°C/W
$R_{th\ j\text{-}amb}$	Thermal Resistance Junction-ambient	Max.	13 (*)	35	°C/W

(*) Mounted on aluminum substrate

PIN FUNCTIONS (refer to the block diagram)

MW.15	PowerSO	Name	Function
1;15	2;19	Sense A; Sense B	Between this pin and ground is connected the sense resistor to control the current of the load.
2;3	4;5	Out 1; Out 2	Outputs of the Bridge A; the current that flows through the load connected between these two pins is monitored at pin 1.
4	6	V_S	Supply Voltage for the Power Output Stages. A non-inductive 100nF capacitor must be connected between this pin and ground.
5;7	7;9	Input 1; Input 2	TTL Compatible Inputs of the Bridge A.
6;11	8;14	Enable A; Enable B	TTL Compatible Enable Input: the L state disables the bridge A (enable A) and/or the bridge B (enable B).
8	1,10,11,20	GND	Ground.
9	12	VSS	Supply Voltage for the Logic Blocks. A100nF capacitor must be connected between this pin and ground.
10; 12	13;15	Input 3; Input 4	TTL Compatible Inputs of the Bridge B.
13; 14	16;17	Out 3; Out 4	Outputs of the Bridge B. The current that flows through the load connected between these two pins is monitored at pin 15.
–	3;18	N.C.	Not Connected

ELECTRICAL CHARACTERISTICS (V_S = 42V; V_{SS} = 5V, T_j = 25°C; unless otherwise specified)

Symbol	Parameter	Test Conditions	Min.	Typ.	Max.	Unit
V_S	Supply Voltage (pin 4)	Operative Condition	V_{IH} +2.5		46	V
V_{SS}	Logic Supply Voltage (pin 9)		4.5	5	7	V
I_S	Quiescent Supply Current (pin 4)	V_{en} = H; I_L = 0 V_i = L V_i = H		13 50	22 70	mA mA
		V_{en} = L V_i = X			4	mA
I_{SS}	Quiescent Current from V_{SS} (pin 9)	V_{en} = H; I_L = 0 V_i = L V_i = H		24 7	36 12	mA mA
		V_{en} = L V_i = X			6	mA
V_{iL}	Input Low Voltage (pins 5, 7, 10, 12)		–0.3		1.5	V
V_{iH}	Input High Voltage (pins 5, 7, 10, 12)		2.3		VSS	V
I_{iL}	Low Voltage Input Current (pins 5, 7, 10, 12)	V_i = L			–10	µA
I_{iH}	High Voltage Input Current (pins 5, 7, 10, 12)	Vi = H ≤ V_{SS} –0.6V		30	100	µA
V_{en} = L	Enable Low Voltage (pins 6, 11)		–0.3		1.5	V
V_{en} = H	Enable High Voltage (pins 6, 11)		2.3		V_{SS}	V
I_{en} = L	Low Voltage Enable Current (pins 6, 11)	V_{en} = L			–10	µA
I_{en} = H	High Voltage Enable Current (pins 6, 11)	V_{en} = H ≤ V_{SS} –0.6V		30	100	µA
$V_{CEsat\ (H)}$	Source Saturation Voltage	I_L = 1A I_L = 2A	0.95	1.35 2	1.7 2.7	V V
$V_{CEsat\ (L)}$	Sink Saturation Voltage	I_L = 1A (5) I_L = 2A (5)	0.85	1.2 1.7	1.6 2.3	V V
V_{CEsat}	Total Drop	I_L = 1A (5) I_L = 2A (5)	1.80		3.2 4.9	V V
V_{sens}	Sensing Voltage (pins 1, 15)		–1 (1)		2	V

ELECTRICAL CHARACTERISTICS (continued)

Symbol	Parameter	Test Conditions	Min.	Typ.	Max.	Unit
T_1 (V_i)	Source Current Turn-off Delay	0.5 V_i to 0.9 I_L (2); (4)		1.5		µs
T_2 (V_i)	Source Current Fall Time	0.9 I_L to 0.1 I_L (2); (4)		0.2		µs
T_3 (V_i)	Source Current Turn-on Delay	0.5 V_i to 0.1 I_L (2); (4)		2		µs
T_4 (V_i)	Source Current Rise Time	0.1 I_L to 0.9 I_L (2); (4)		0.7		µs
T_5 (V_i)	Sink Current Turn-off Delay	0.5 V_i to 0.9 I_L (3); (4)		0.7		µs
T_6 (V_i)	Sink Current Fall Time	0.9 I_L to 0.1 I_L (3); (4)		0.25		µs
T_7 (V_i)	Sink Current Turn-on Delay	0.5 V_i to 0.9 I_L (3); (4)		1.6		µs
T_8 (V_i)	Sink Current Rise Time	0.1 I_L to 0.9 I_L (3); (4)		0.2		µs
fc (V_i)	Commutation Frequency	I_L = 2A		25	40	KHz
T_1 (V_{en})	Source Current Turn-off Delay	0.5 V_{en} to 0.9 I_L (2); (4)		3		µs
T_2 (V_{en})	Source Current Fall Time	0.9 I_L to 0.1 I_L (2); (4)		1		µs
T_3 (V_{en})	Source Current Turn-on Delay	0.5 V_{en} to 0.1 I_L (2); (4)		0.3		µs
T_4 (V_{en})	Source Current Rise Time	0.1 I_L to 0.9 I_L (2); (4)		0.4		µs
T_5 (V_{en})	Sink Current Turn-off Delay	0.5 V_{en} to 0.9 I_L (3); (4)		2.2		µs
T_6 (V_{en})	Sink Current Fall Time	0.9 I_L to 0.1 I_L (3); (4)		0.35		µs
T_7 (V_{en})	Sink Current Turn-on Delay	0.5 V_{en} to 0.9 I_L (3); (4)		0.25		µs
T_8 (V_{en})	Sink Current Rise Time	0.1 I_L to 0.9 I_L (3); (4)		0.1		µs

1) 1)Sensing voltage can be –1 V for t ≤ 50 µsec; in steady state V_{sens} min ≥ – 0.5 V.
2) See fig. 2.
3) See fig. 4.
4) The load must be a pure resistor.

Figure 1 : Typical Saturation Voltage vs. Output Current.

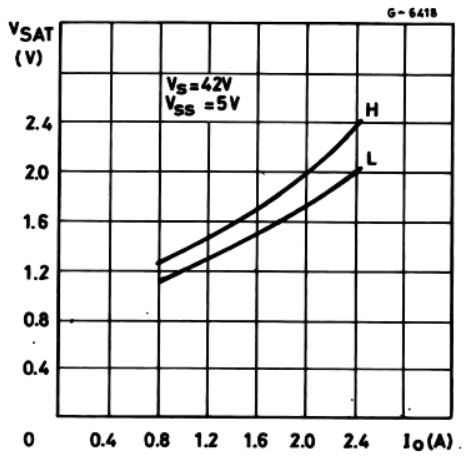

Figure 2 : Switching Times Test Circuits.

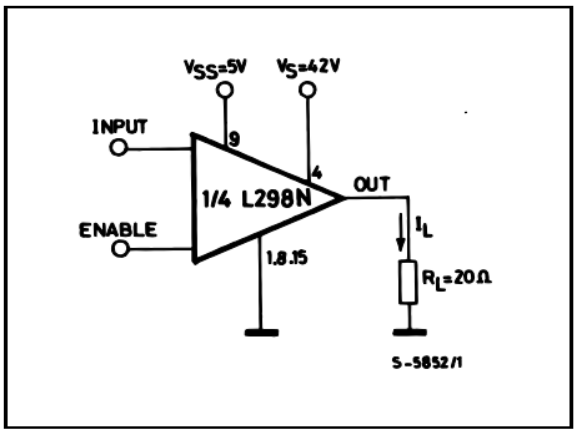

Note : For INPUT Switching, set EN = H
For ENABLE Switching, set IN = H

Figure 3 : Source Current Delay Times vs. Input or Enable Switching.

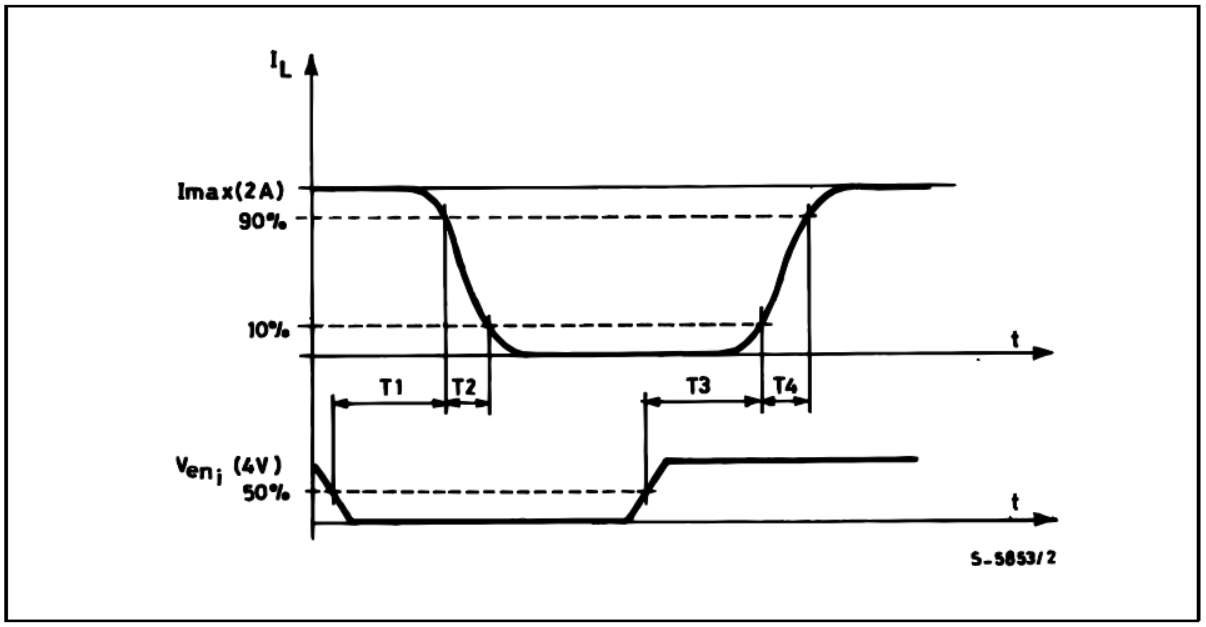

Figure 4 : Switching Times Test Circuits.

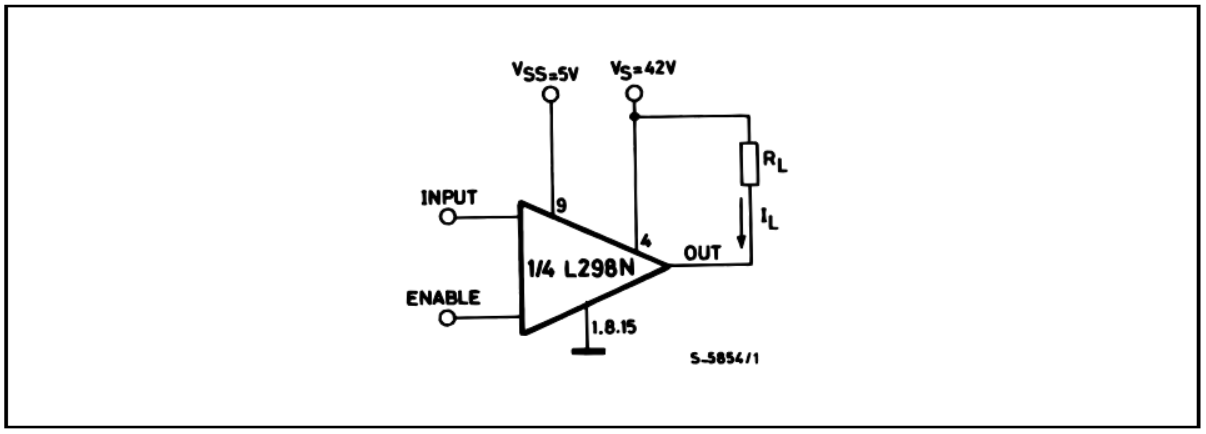

Note : For INPUT Switching, set EN = H
For ENABLE Switching, set IN = L

Figure 5 : Sink Current Delay Times vs. Input 0 V Enable Switching.

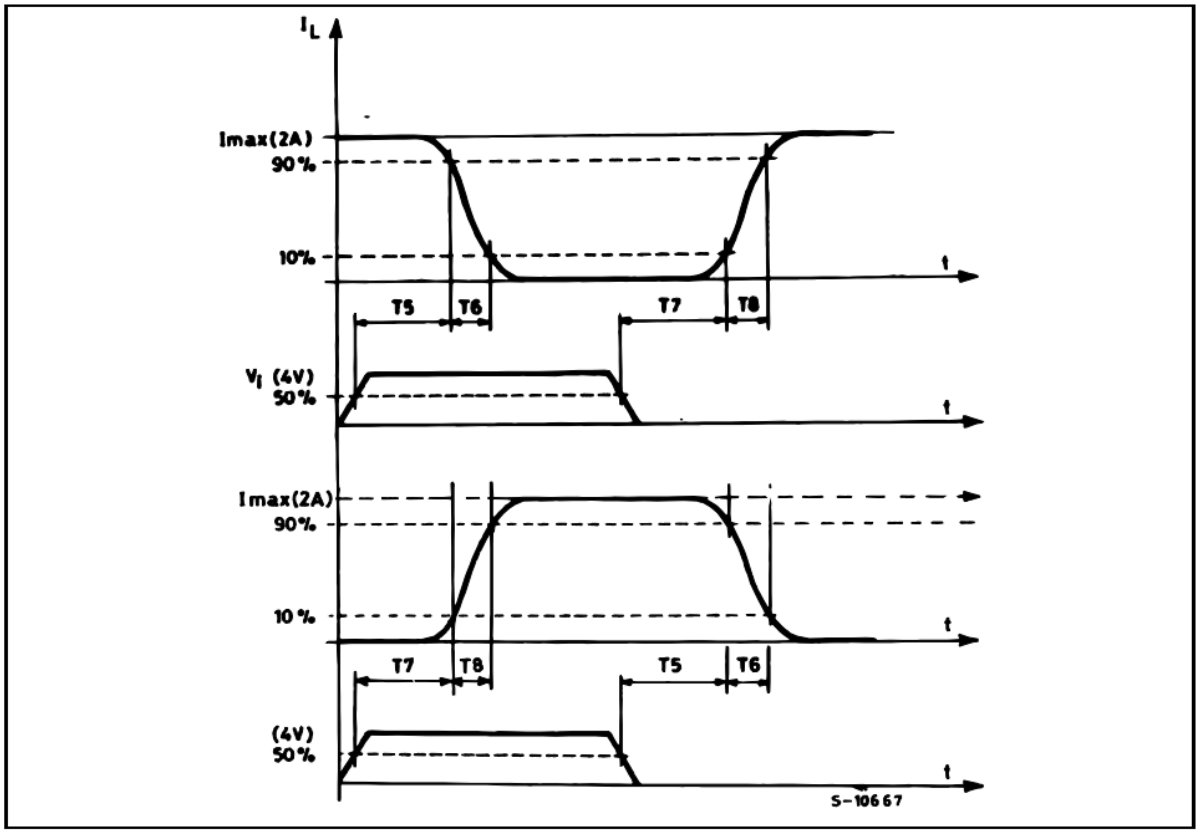

Figure 6 : Bidirectional DC Motor Control.

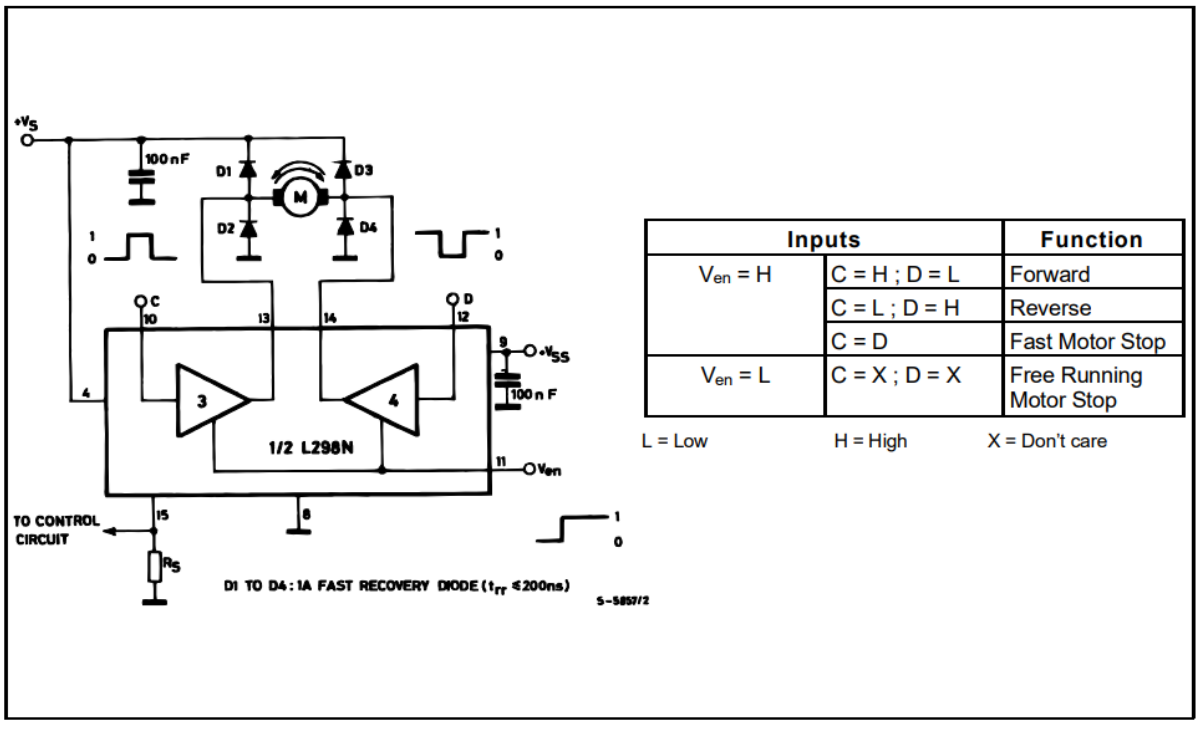

Inputs		Function
V_{en} = H	C = H ; D = L	Forward
	C = L ; D = H	Reverse
	C = D	Fast Motor Stop
V_{en} = L	C = X ; D = X	Free Running Motor Stop

L = Low H = High X = Don't care

Figure 7 : For higher currents, outputs can be paralleled. Take care to parallel channel 1 with channel 4 and channel 2 with channel 3.

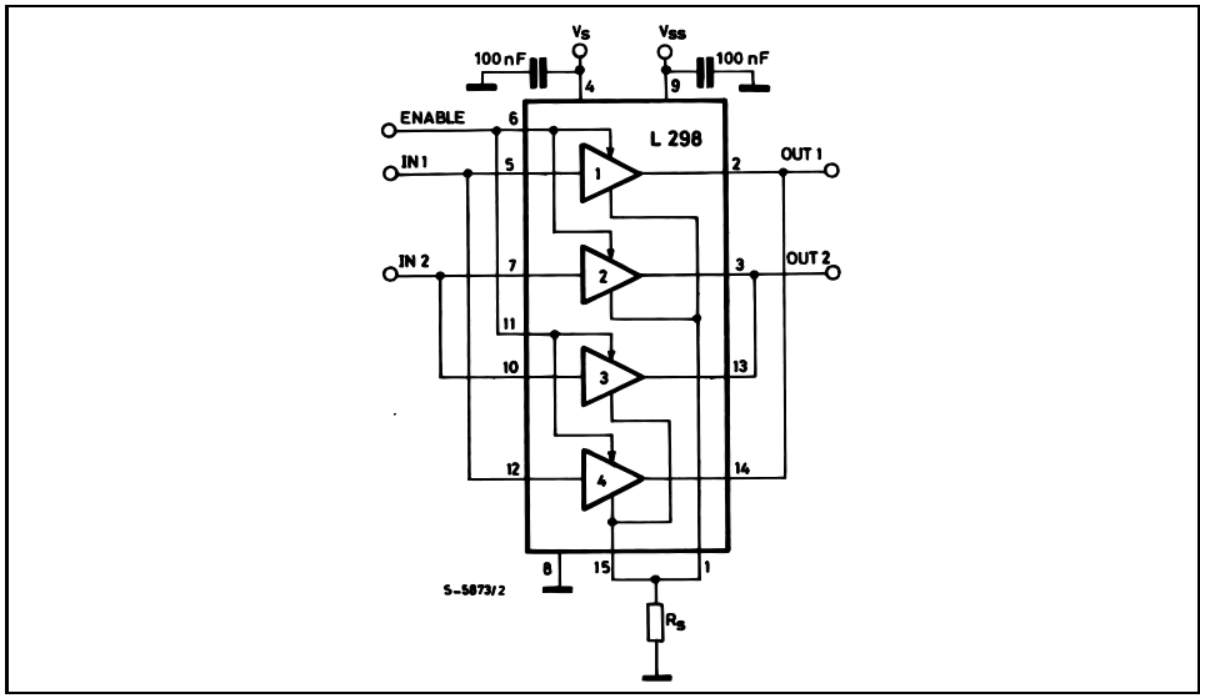

APPLICATION INFORMATION (Refer to the block diagram)

1.1. POWER OUTPUT STAGE

The L298 integrates two power output stages (A ; B). The power output stage is a bridge configuration and its outputs can drive an inductive load in common or differenzial mode, depending on the state of the inputs. The current that flows through the load comes out from the bridge at the sense output : an external resistor (R_{SA} ; R_{SB}.) allows to detect the intensity of this current.

1.2. INPUT STAGE

Each bridge is driven by means of four gates the input of which are In1 ; In2 ; EnA and In3 ; In4 ; EnB. The In inputs set the bridge state when The En input is high ; a low state of the En input inhibits the bridge. All the inputs are TTL compatible.

2. SUGGESTIONS

A non inductive capacitor, usually of 100 nF, must be foreseen between both Vs and Vss, to ground, as near as possible to GND pin. When the large capacitor of the power supply is too far from the IC, a second smaller one must be foreseen near the L298.

The sense resistor, not of a wire wound type, must be grounded near the negative pole of Vs that must be near the GND pin of the I.C.

Each input must be connected to the source of the driving signals by means of a very short path.

Turn-On and Turn-Off : Before to Turn-ON the Supply Voltage and before to Turn it OFF, the Enable input must be driven to the Low state.

3. APPLICATIONS

Fig 6 shows a bidirectional DC motor control Schematic Diagram for which only one bridge is needed. The external bridge of diodes D1 to D4 is made by four fast recovery elements (trr $\leq$ 200 nsec) that must be chosen of a VF as low as possible at the worst case of the load current.

The sense output voltage can be used to control the current amplitude by chopping the inputs, or to provide overcurrent protection by switching low the enable input.

The brake function (Fast motor stop) requires that the Absolute Maximum Rating of 2 Amps must never be overcome.

When the repetitive peak current needed from the load is higher than 2 Amps, a paralleled configuration can be chosen (See Fig.7).

An external bridge of diodes are required when inductive loads are driven and when the inputs of the IC are chopped ; Shottky diodes would be preferred.

This solution can drive until 3 Amps In DC operation and until 3.5 Amps of a repetitive peak current.

On Fig 8 it is shown the driving of a two phase bipolar stepper motor ; the needed signals to drive the inputs of the L298 are generated, in this example, from the IC L297.

Fig 9 shows an example of P.C.B. designed for the application of Fig 8.

Fig 10 shows a second two phase bipolar stepper motor control circuit where the current is controlled by the I.C. L6506.

Figure 8 : Two Phase Bipolar Stepper Motor Circuit.

This circuit drives bipolar stepper motors with winding currents up to 2 A. The diodes are fast 2 A types.

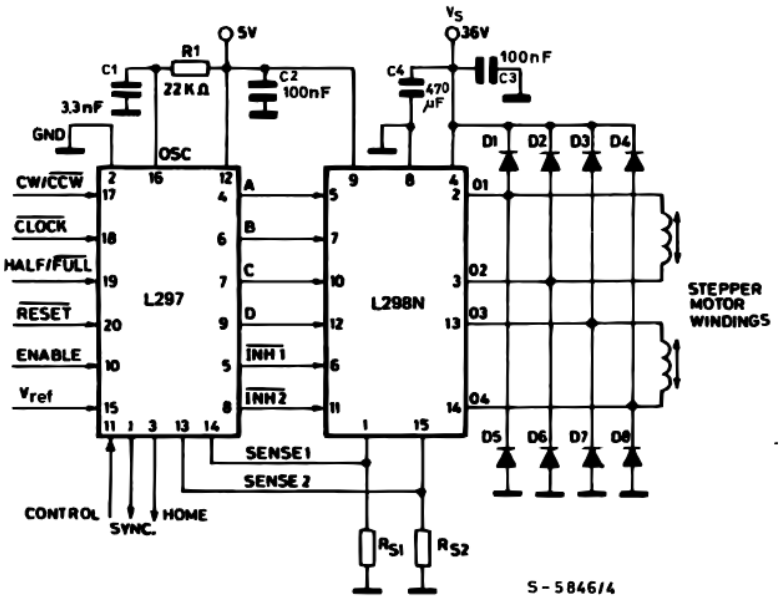

$R_{S1} = R_{S2} = 0.5\ \Omega$

D1 to D8 = 2 A Fast diodes { $V_F \leq 1.2$ V @ I = 2 A ; trr ≤ 200 ns

Figure 9 : Suggested Printed Circuit Board Layout for the Circuit of fig. 8 (1:1 scale).

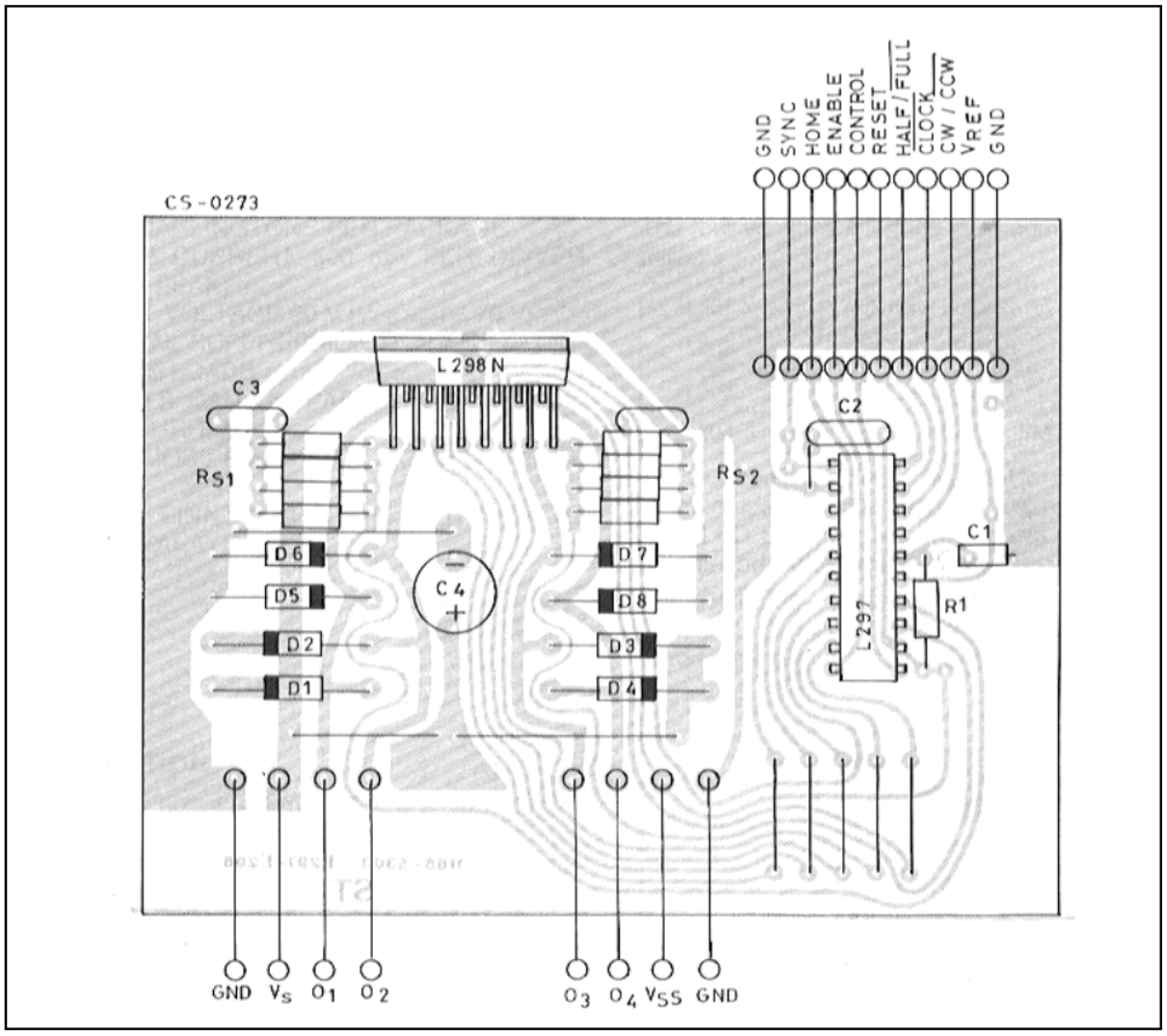

Figure 10 : Two Phase Bipolar Stepper Motor Control Circuit by Using the Current Controller L6506.

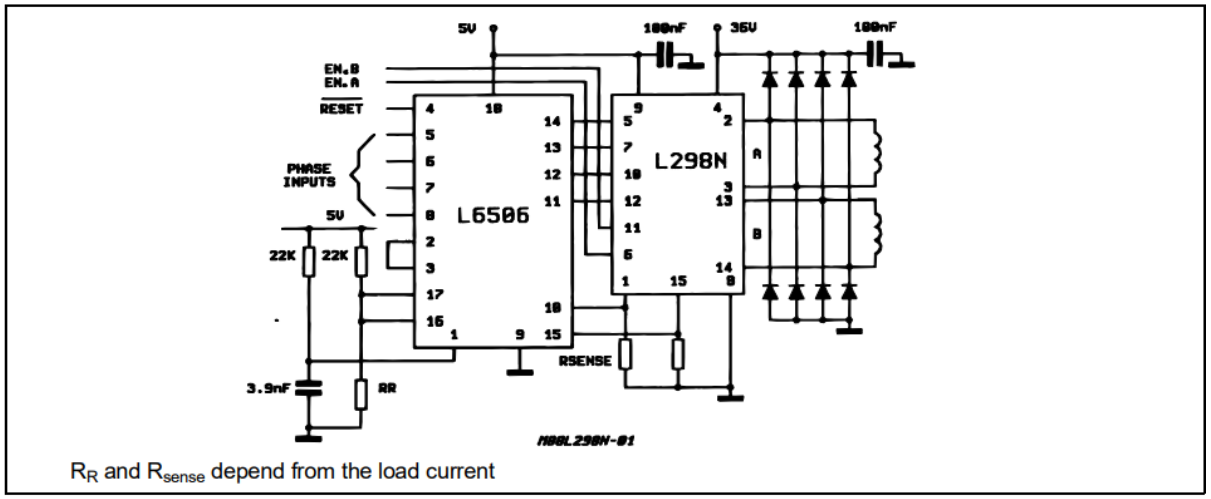

R_R and R_{sense} depend from the load current

DIM.	mm			inch		
	MIN.	TYP.	MAX.	MIN.	TYP.	MAX.
A			5			0.197
B			2.65			0.104
C			1.6			0.063
D		1			0.039	
E	0.49		0.55	0.019		0.022
F	0.66		0.75	0.026		0.030
G	1.02	1.27	1.52	0.040	0.050	0.060
G1	17.53	17.78	18.03	0.690	0.700	0.710
H1	19.6			0.772		
H2			20.2			0.795
L	21.9	22.2	22.5	0.862	0.874	0.886
L1	21.7	22.1	22.5	0.854	0.870	0.886
L2	17.65		18.1	0.695		0.713
L3	17.25	17.5	17.75	0.679	0.689	0.699
L4	10.3	10.7	10.9	0.406	0.421	0.429
L7	2.65		2.9	0.104		0.114
M	4.25	4.55	4.85	0.167	0.179	0.191
M1	4.63	5.08	5.53	0.182	0.200	0.218
S	1.9		2.6	0.075		0.102
S1	1.9		2.6	0.075		0.102
Dia1	3.65		3.85	0.144		0.152

OUTLINE AND MECHANICAL DATA

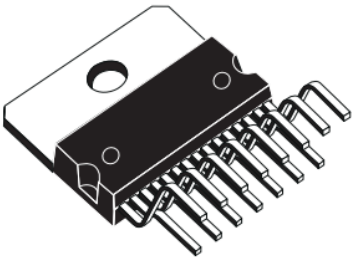

Multiwatt15 V

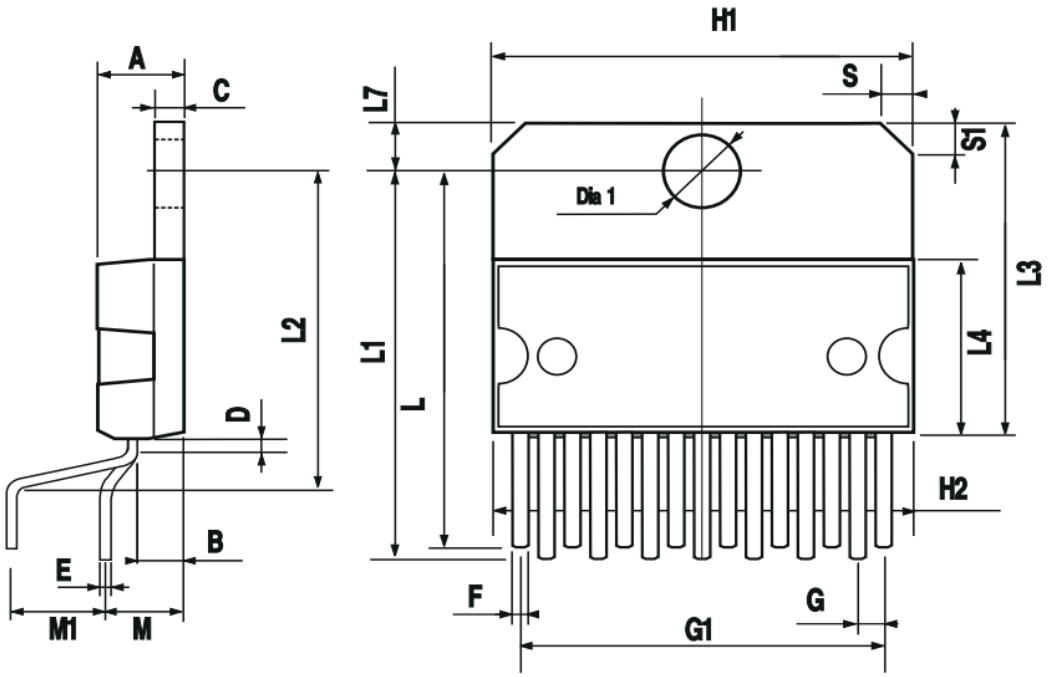

DIM.	mm			inch		
	MIN.	TYP.	MAX.	MIN.	TYP.	MAX.
A			5			0.197
B			2.65			0.104
C			1.6			0.063
E	0.49		0.55	0.019		0.022
F	0.66		0.75	0.026		0.030
G	1.14	1.27	1.4	0.045	0.050	0.055
G1	17.57	17.78	17.91	0.692	0.700	0.705
H1	19.6			0.772		
H2			20.2			0.795
L		20.57			0.810	
L1		18.03			0.710	
L2		2.54			0.100	
L3	17.25	17.5	17.75	0.679	0.689	0.699
L4	10.3	10.7	10.9	0.406	0.421	0.429
L5		5.28			0.208	
L6		2.38			0.094	
L7	2.65		2.9	0.104		0.114
S	1.9		2.6	0.075		0.102
S1	1.9		2.6	0.075		0.102
Dia1	3.65		3.85	0.144		0.152

OUTLINE AND MECHANICAL DATA

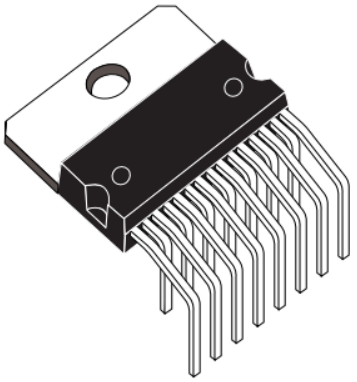

Multiwatt15 H

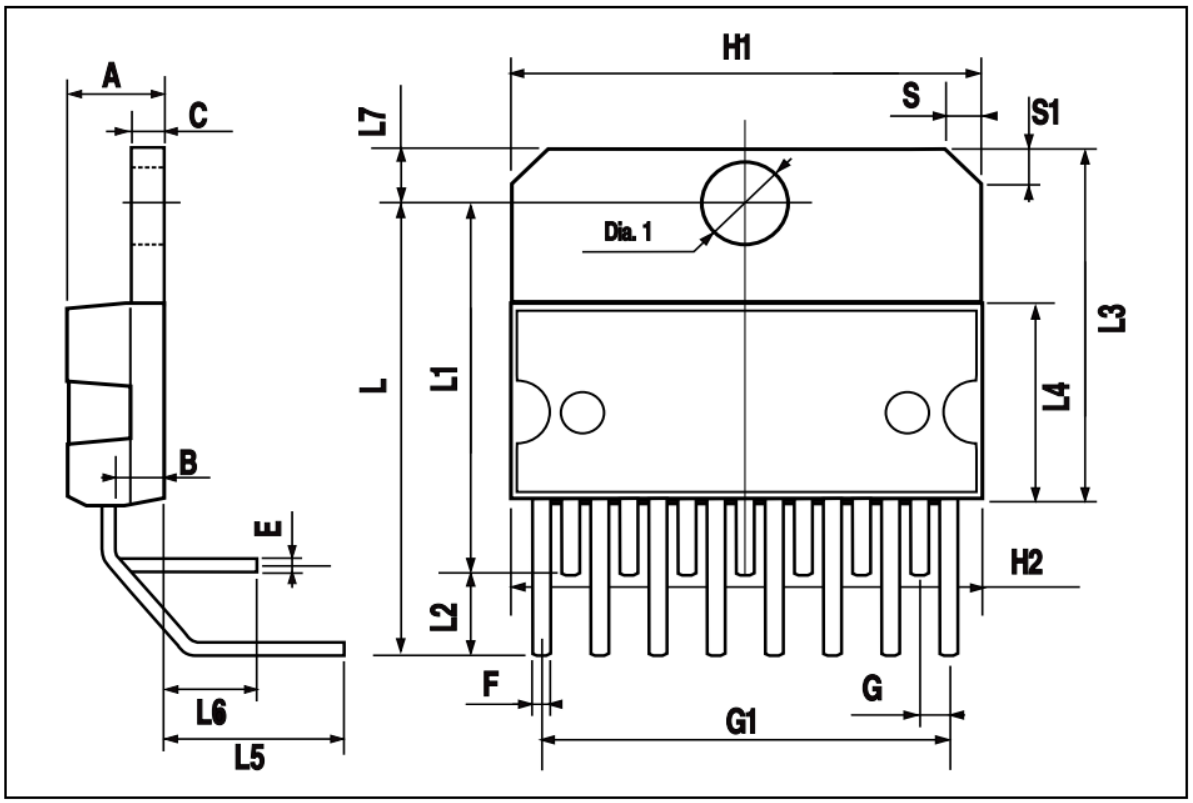

DIM.	mm			inch		
	MIN.	TYP.	MAX.	MIN.	TYP.	MAX.
A			3.6			0.142
a1	0.1		0.3	0.004		0.012
a2			3.3			0.130
a3	0		0.1	0.000		0.004
b	0.4		0.53	0.016		0.021
c	0.23		0.32	0.009		0.013
D (1)	15.8		16	0.622		0.630
D1	9.4		9.8	0.370		0.386
E	13.9		14.5	0.547		0.570
e		1.27			0.050	
e3		11.43			0.450	
E1 (1)	10.9		11.1	0.429		0.437
E2			2.9			0.114
E3	5.8		6.2	0.228		0.244
G	0		0.1	0.000		0.004
H	15.5		15.9	0.610		0.626
h			1.1			0.043
L	0.8		1.1	0.031		0.043
N	10° (max.)					
S	8° (max.)					
T		10			0.394	

(1) "D and F" do not include mold flash or protrusions.
- Mold flash or protrusions shall not exceed 0.15 mm (0.006").
- Critical dimensions: "E", "G" and "a3"

OUTLINE AND MECHANICAL DATA

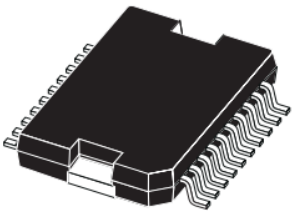

JEDEC MO-166

PowerSO20

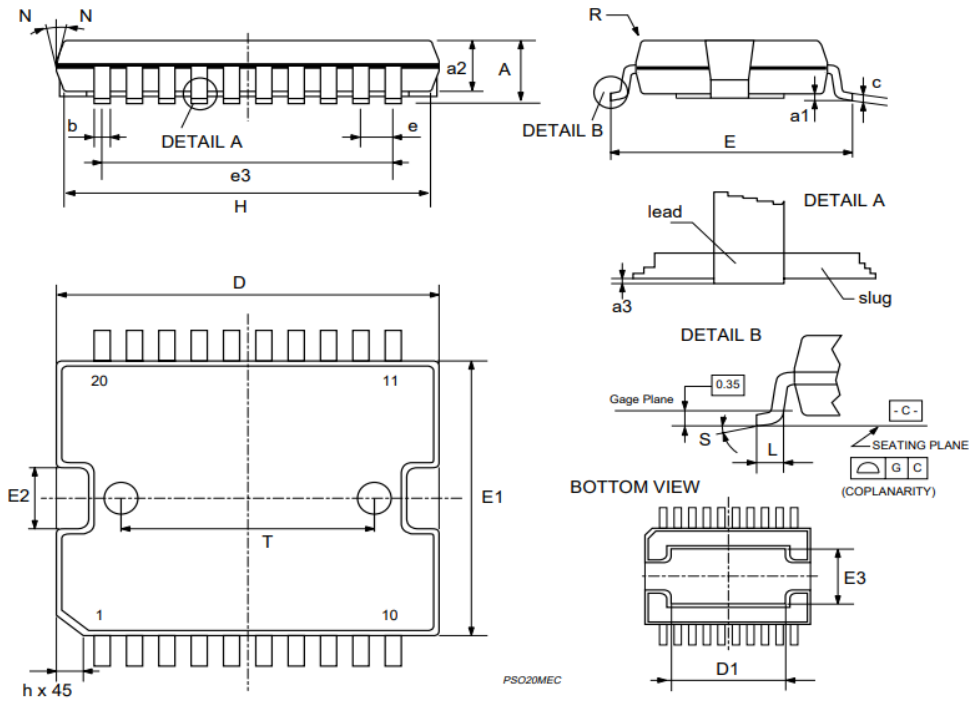

Information furnished is believed to be accurate and reliable. However, STMicroelectronics assumes no responsibility for the consequences of use of such information nor for any infringement of patents or other rights of third parties which may result from its use. No license is granted by implication or otherwise under any patent or patent rights of STMicroelectronics. Specification mentioned in this publication are subject to change without notice. This publication supersedes and replaces all information previously supplied. STMicroelectronics products are not authorized for use as critical components in life support devices or systems without express written approval of STMicroelectronics.

The ST logo is a registered trademark of STMicroelectronics

© 2000 STMicroelectronics – Printed in Italy – All Rights Reserved

STMicroelectronics GROUP OF COMPANIES

Australia - Brazil - China - Finland - France - Germany - Hong Kong - India - Italy - Japan - Malaysia - Malta - Morocco - Singapore - Spain - Sweden - Switzerland - United Kingdom - U.S.A.

http://www.st.com